

# JGR Space Physics



## RESEARCH ARTICLE

10.1029/2020JA028598

### Key Points:

- Digisonde data and modeling results are used to study the disturbed electric field influence in the Es layer formation
- The electric fields and Es layers are analyzed during days around 20 magnetic storms for regions near the geographic/magnetic equator and for a low-latitude station
- The results show that the electric field influence in Es layer development depends on the region's characteristics

### Supporting Information:

- Supporting Information S1

### Correspondence to:

L. C. A. Resende,  
[laysa.resende@gmail.com](mailto:laysa.resende@gmail.com);  
[laysa.resende@inpe.br](mailto:laysa.resende@inpe.br)

### Citation:

Resende, L. C. A., Shi, J., Denardini, C. M., Batista, I. S., Picanço, G. A. S., Moro, J., et al. (2021). The impact of the disturbed electric field in the sporadic E (Es) layer development over Brazilian region. *Journal of Geophysical Research: Space Physics*, 126, e2020JA028598. <https://doi.org/10.1029/2020JA028598>






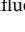








Received 22 AUG 2020

Accepted 24 JAN 2021

© 2021. The Authors.

This is an open access article under the terms of the [Creative Commons Attribution License](https://creativecommons.org/licenses/by/4.0/), which permits use, distribution and reproduction in any medium, provided the original work is properly cited.

## The Impact of the Disturbed Electric Field in the Sporadic E (Es) Layer Development Over Brazilian Region

L. C. A. Resende<sup>1,2</sup> , J. Shi<sup>1,3</sup> , C. M. Denardini<sup>2</sup> , I. S. Batista<sup>2</sup> , G. A. S. Picanço<sup>2</sup> , J. Moro<sup>1,5</sup> , R. A. J. Chagas<sup>2</sup> , D. Barros<sup>2</sup> , S. S. Chen<sup>2</sup> , P. A. B. Nogueira<sup>4</sup> , V. F. Andrioli<sup>1,2</sup> , R. P. Silva<sup>2</sup> , A. J. Carrasco<sup>2,6</sup> , R. C. de Araujo<sup>7</sup>, C. Wang<sup>1</sup> , and Z. Liu<sup>1</sup>

<sup>1</sup>State Key Laboratory of Space Weather, NSSC/CAS, Beijing, China, <sup>2</sup>National Institute for Space Research—INPE/MCTI, São José dos Campos, Brazil, <sup>3</sup>University of Chinese Academy of Sciences, Beijing, China, <sup>4</sup>Federal Institute of Education, Science and Technology of São Paulo, Jacarei, Brazil, <sup>5</sup>Southern Space Coordination, COESU/INPE-MCTI, Santa Maria, Brazil, <sup>6</sup>University of Los Andes, Mérida, Venezuela, <sup>7</sup>Departamento de Física, Universidade Federal de Roraima, Boa Vista, Brasil

**Abstract** During disturbed periods, E region electric fields can cause anomalous Es layer behavior, which is observed in the digital ionosonde data. To investigate the influence of these electric fields in the Es layer development, we analyzed a set of 20 magnetic storms from 2015 to 2018 over Boa Vista (BV, 2.8°N, 60.7°W, dip ~18°), São Luís (SLZ, 2.3°S, 44.2°W, dip ~8°), and Cachoeira Paulista (CXP, 22.41°S, 45°W, dip ~35°). The electric field zonal components during the main and recovery phases of each magnetic storm are computed to study the corresponding characteristics of these Es seen in ionograms. Additionally, a numerical model (MIRE, Portuguese acronym for E Region Ionospheric Model) is used to analyze the Es layer dynamics modification around disturbed times. Using observation data and simulations, we were able to establish a threshold value for the electric field intensity for each region that can affect the Es layer formation. The results sustain that the strong Es layer in BV can be an indicator of the disturbed dynamo event. At SLZ, on the other hand, the Es layers are affected by the competition mechanisms of their formation, as equatorial electrojet irregularities and winds, during the main phase of the magnetic storm. Over CXP, the Es layer dynamics are dominated by the wind shear mechanism. Finally, this study provides new insights into the real impact of the electric field in the Es layer development over the Brazilian sector. Thus, our results lead to a better understanding of the underlying mechanisms related to the Es layer formation and dynamics.

## 1. Introduction

The dynamics of the sporadic E (Es) layers at low/middle latitudes are well-known in the literature (Kopp, 1997; Mathews, 1998; Prasad et al., 2012; Resende et al. 2013, 2017a; Whitehead, 1961). These layers are characterized by patches of enhanced electron density around 100 km in the ionosphere, composed mainly of metallic ions, such as Mg<sup>+</sup> and Fe<sup>+</sup>. They are classified into several types according to the physical form in their observations (Layzer, 1972).

The three main categories of Es layers (equatorial, mid/low-latitude, and auroral) are readily distinguishable in ionograms by letters. The middle and low latitude Es layers are defined as type “c” (cusp), “h” (high), and “l (low)/f” (flat). These types of Es layers are controlled by tidal winds due to the vertical wind shear process (Haldoupis, 2011). In middle latitudes, Pignalberi et al. (2014) using the Height-Time-Intensity (HTI) technique shows that these Es layers have a well-defined semidiurnal periodicity during the summer while a diurnal behavior is present in August and September months. On the other hand, Resende et al. (2017a) found that the diurnal component of the tidal wind is the most important to form Es layer at low latitudes. At auroral latitudes the Es layer is denoted as Es<sub>a</sub> or type “a,” and it is associated with particle precipitation. However, the Es<sub>a</sub> layers also are identified in ionograms over the Brazilian sector which is under the influence of the South America Magnetic Anomaly (SAMA) (Batista & Abdu, 1977).

In magnetic equatorial regions, the Equatorial Electrojet Current (EEJ) plasma instabilities, mainly the Gradient Drift instability (Type II irregularities) driven by the vertical polarization electric field, produce

a diffuse and non-blanketing Es trace named  $Es_q$  (equatorial) layers (Chandra & Rastogi, 1975; Denardini et al., 2016; Resende et al., 2016; Moro et al., 2017). The signatures of the  $Es_q$  layers appear as a scattering of the radio wave signal that covers most of the low-frequency scale and occurs very regularly when the polarization electric field and density gradient is well set at the E region heights (Resende et al., 2013). It is important to mention that in the vicinity of the magnetic equator, the wind shear mechanism is not effective due to the horizontal configuration of the magnetic field, not allowing the denser/blanketing layer formation in the E region.

The Es layer around the globe can suffer significant modifications due to the ionospheric electric field, mainly at locations near the geographic and magnetic equator. Resende et al. (2016) studied the competition between tidal winds and electric fields in the formation of blanketing sporadic E layers during quiet periods over São Luís, a region of transition from equatorial to low latitude due to an apparent northward movement of the magnetic equator. The authors showed that the blanketing sporadic E layers occur due to the vertical electric field weakening, caused by the departure of the magnetic equator from São Luís. Therefore, the tidal winds are more effective during some hours, forming denser Es layers. In other words, the vertical electric field component is responsible for Type II irregularity, and, consequently, for the  $Es_q$  occurrence. Thus, when this electric field component is low, the wind shear mechanism becomes dominant. The same kind of analysis was performed by Moro et al. (2017) during disturbed periods, in which the authors found similar results about the relationship between the vertical electric field and blanketing Es layers. Hence, the blanketing Es layers occurrence at equatorial regions depends on the electric field vertical component.

Abdu et al. (2003), Carrasco et al. (2007), and Abdu and Brum (2009) showed that the equatorial electric field during the evening pre-reversal enhancement (PRE) can cause Es layer intensification or disruption at low latitudes. The vertical electric field mapped from the equatorial F region to low latitudes can have some influence on the Es layer formation. These modifications in the PRE can be caused by an enhancement in the conductivity gradient near sunset due to the upward propagating planetary waves and tidal modes (Abdu & Brum, 2009; Abdu et al., 2006; Pancheva et al., 2003).

Recent studies have shown that the disturbed electric fields have some influence in the Es layer structures during geomagnetic storms. For instance, Abdu et al. (2014) reported on intensification or disruption of the Es layers associated with the Hall electric field induced by the prompt penetration electric fields (PPEFs) at low latitudes. More recently, Resende et al. (2020) detected strong Es layers in Boa Vista (BV, Geographic Coordinates: 2.8°N, 60.7°W, Magnetic Inclination:  $\sim 18^\circ$ ), a station located near the geographic equator in the Brazilian sector, during the recovery phase of magnetic storms. They concluded that these anomalous Es layers are a consequence of the combined effect of the winds and disturbed electric fields. The authors concluded that the zonal westward electric field in the ionosphere due to the disturbance dynamo effect (DDEF) is the probable cause of such Es layer intensification over BV. However, since the disturbance dynamo is a global mechanism, these strong Es layers would also be expected in other regions. Since they did not observe this fact, they concluded that the real consequence of the electric field in the formation of Es layers during the disturbed periods was still unclear.

In light of the above discussion, this work analyses the electric field role in the Es layer formation during magnetic storms, providing novel insights about their coupling. First, we analyzed a set of days around 20 magnetic storms in three different regions over the Brazilian sector: an equatorial geographic station (BV), a transition station from equatorial to low latitude (São Luís (SLZ), Geographic Coordinates: 2.3°S, 44.2°W, Magnetic Inclination:  $\sim 8^\circ$ ), and a low latitude station (Cachoeira Paulista (CXP), Geographic Coordinates: 22.41°S, 45°W, Magnetic Inclination:  $\sim 35^\circ$ ). Afterward, we performed an in-depth analysis of the F region parameters to obtain the electric field values. Hence, it was possible to quantify the effect of the electric field in the Es layer formation for each analyzed region. The estimated electric fields were used as input to the E region ionospheric model (MIRE) (Resende et al., 2017a) to find the threshold value that is capable to cause the Es layer strengthening. Therefore, all this analysis allowed us to discuss the electric field role in the Es layer dynamics considering different locations during the disturbed periods, as shown in the following sections.

## 2. Methodology

Data from digital ionosondes and MIRE simulations were used to study the effect of the electric fields in the Es layer modification during 20 geomagnetic storms between 2015 and 2018. The methodology of the analysis is presented in the following sections.

### 2.1. Analysis of the Vertical Drift and Es Layer Parameters

We used the data obtained from the digital ionosondes (Digisonde) installed in BV, SLZ, and CXP to collect the F region and Es layer parameters. This radar transmits radio waves continuously into the ionosphere ranging from 1 to 30 MHz (Reinisch et al., 2009).

The vertical drift velocity ( $V_z$ ) is calculated as  $\Delta hF/\Delta t$  where  $hF$  is the true height, corresponding to a defined frequency, obtained by the vertical electron density profiles of two consecutive ionograms, being  $\Delta t$  the time interval between them. The frequencies at 4, 5, and 6 MHz were chosen for the calculation and the average was considered representative of  $V_z$  (Abdu et al., 2010), which represents the vertical plasma drift over the magnetic equatorial regions. Since the three regions used in the present study are located a little outside (BV and SLZ) or far away (CXP) from the magnetic equator, it is necessary to consider the effect of the meridional wind in the vertical plasma motion (Rishbeth et al., 1978). Therefore,  $V_z$  depends on the apparent vertical drifts ( $V_{ap}$ ) (Nogueira et al., 2011). Furthermore, the recombination processes need to be taken into account for the drift velocity calculation since the F layer can be located at heights lower than 300 km (Bittencourt & Abdu, 1981). Thus, the final vertical drift ( $V_{zf}$ ) and  $V_{ap}$  are obtained as follows:

$$V_{zf} = V_{ap} - \beta H, \quad (1)$$

$$V_{ap} = V_z \cdot \cos I \pm U_F \cdot \cos I \cdot \sin I - w_D \cdot \sin^2 I, \quad (2)$$

where the  $\beta$  is the recombination coefficient,  $H$  is the scale height of ionization,  $I$  is the magnetic inclination angle ( $\sim 18^\circ$  in BV,  $\sim 7^\circ$  in SLZ,  $\sim 35^\circ$  in CXP),  $U_F$  is the meridional wind component in the F region (positive northward), and  $w_D$  is the contribution of diffusion to the vertical plasma velocity given by equation  $w_D = g / \nu_i$ , in which  $g$  is the gravity acceleration, and  $\nu_i$  is the ion-neutral collision frequency. A detailed methodology to obtain these parameters is described in Nogueira et al. (2011) and Resende et al. (2020).

Other three parameters were also necessary to analyze the electric field effect in the Es layer behavior: the virtual height of the F region ( $h'F$  in km), the Es blanketing frequency ( $fbEs$ ), which corresponds to the frequency up to which the Es layer blocks the transmitted electromagnetic signal, and the top frequency ( $ftEs$ ), which is the maximum frequency reflected by the Es layer. The frequency parameters are given in MHz. Additionally, we manually checked all the parameters used in this analysis to obtain a reliable ionospheric profile (Reinisch et al., 2004) since significant discrepancies are often found between the automatically generated and real ionospheric parameters in the studied regions.

### 2.2. The E Region Ionospheric Model—MIRE

MIRE is used to study the Es layer behavior at equatorial and low latitudes over the Brazilian sector (Carasco et al., 2007; Resende et al. 2016, 2017a, 2017b). The electron density

$$ne = [O_2^+] + [NO^+] + [O^+] + [N_2^+] + [Fe^+] + [Mg^+], \quad (3)$$

is computed using the equations of continuity and momentum for the molecular/atomic ions ( $NO^+$ ,  $O_2^+$ ,  $N_2^+$ ,  $O^+$ ) and metallic ions ( $Fe^+$ ,  $Mg^+$ ). The system is solved using 0.05 km grid spacing in height, and 1 min time step between 00 UT and 24 UT.

The transport term of the continuity equation depends mainly on the meridional ( $U_x$ ) and zonal ( $U_y$ ) components of the tidal winds and the electric field components ( $E_{x,y,z}$ ) as follows

$$V_{iz} = \frac{\omega_i^2}{(v_{in}^2 + \omega_i^2)} \left[ \cos I \cdot \sin I \cdot U_x + \frac{v_{in}}{\omega_i} \cdot \cos I \cdot U_y + \frac{1}{v_{in}} \frac{e}{m_i} \cdot \cos I \cdot \sin I \cdot \left( E_x + \frac{e}{\omega_i m_i} \cdot \cos I \cdot E_y + \frac{e}{v_{in} m_i} \cdot \left( \frac{v_{in}^2}{\omega_i^2} + \sin^2 I \right) \cdot E_z \right) \right], \quad (4)$$

where  $\omega_i$  is ion gyrofrequency,  $v_{in}$  is the ion-neutral collision frequency,  $m_i$  is the mass of the ion, and  $e$  is the electric charge of the ion. Regarding the frame of reference, the  $X$ -axis points toward the south; the  $Y$ -axis points toward the east; and the  $Z$ -axis completes the right-handed coordinate system, pointing up.

The wind profile used as input to MIRE was obtained from the last version of the Global Scale Wave Model (GSWM-00). This wind model is derived from the resolution of the Navier-Stokes equations for tidal and planetary wave perturbations as a function of latitude and altitude, for a specific wave periodicity and zonal wavenumber (Hagan et al., 2002; Manson et al., 2002). Therefore, the GSWM-00 successfully describes the wind dynamics until 125 km, which predicts the diurnal (24 h) and the semidiurnal (12 h) tides that are necessary for the Es layer formation in MIRE. The parameters of the GSWM-00 are given by the High-Altitude Observatory of the National Center for Atmospheric Research in Colorado (<http://www.hao.ucar.edu/modeling/gswm/gswm.html>).

Resende et al. (2020) implemented the GSWM-00 parameters in MIRE to analyze the Es layers in BV. In the present study, we extended a similar analysis for SLZ and CXP using the GSWM-00 already included in the MIRE model for the first time for these regions. The horizontal tidal amplitudes ( $U_{x0}(z)$ ,  $U_{y0}(z)$ ), the phases ( $t_{x0}(z)$ ,  $t_{y0}(z)$ ), and the vertical wavelength ( $\lambda_x$ ,  $\lambda_y$ ) of the respective diurnal ( $T = 24$  h) and semidiurnal ( $T = 12$  h) tides as provided by the GSWM-00 are used in the wind shear equations:

$$U_x(z) = U_{x0}(z) \cdot \cos\left(\frac{2\pi}{\lambda_x}(z - z_0) + \frac{2\pi}{T}(t - t_{x0}(z))\right), \quad (5)$$

$$U_y(z) = -U_{y0}(z) \cdot \sin\left(\frac{2\pi}{\lambda_y}(z - z_0) + \frac{2\pi}{T}(t - t_{y0}(z))\right), \quad (6)$$

where the subscripts  $x$  and  $y$  refer to the meridional and zonal directions, respectively,  $z_0$  is a reference height, assumed as 100 km (Mathews & Bekey, 1979; Resende et al., 2017a).

Finally, to perform the electric field effects analysis, we used the relationship that each variation of  $\sim 40$  m/s in the vertical drift velocity obtained in Equation 1 equals to the 1 mV/m in the zonal electric field (Fejer & Scherliess, 1995).

### 2.3. Five Stages of Data Processing

We used the Dst index to identify the geomagnetic storm periods. This data was acquired from the World Data Center in Kyoto (<http://wdc.kugi.kyoto-u.ac.jp/dstae/index.html>). We analyzed a set of 20 moderate/intense magnetic storms ( $\text{Dst} < -50$  nT) that occurred in 2015, 2016, 2017, and 2018. The analysis of this study consisted of:

- identifying the presence of strong Es layers in the ionograms over BV station
- analyzing the ionogram data available for the SLZ and CXP for the same period in the previous step
- excluding the cases of  $\text{Es}_c$  and  $\text{Es}_h$  layers since they are formed only by the wind shear mechanism
- identifying the magnetic storm phase in which the strong Es layers occurred for each region; and
- obtaining the time variation of  $fbEs$  and  $ftEs$  from each selected period.

Table 1 summarizes the data obtained using the described methodology. In this table, we show the quiet day used as reference, the maximum  $ftEs$  observed in this quiet day, the day of geomagnetic storm onset, the level of the magnetic storm represented by the Dst index, the maximum  $ftEs$  for each region together with the day that it was observed, and the magnetic storm phase in which these atypical Es layers occurred.

**Table 1**

List of the Quiet Days Used as a Reference in This Work With the Corresponding Maximum  $fE_s$  Values, the Characteristics of Moderate/Intense Magnetic Storms From 2015 up to 2018 ( $Dst < -50$ ), and the Maximum of the  $fE_s$  Parameter Occurrences Associated With the Magnetic Storm Phase Over BV, SLZ, and CXP stations.

Quiet day	Maximum $fE_{s_{quiet}}$ (MHz)	Magnetic storm	Minimum Dst (nT)	Maximum $fE_{s_{Dist}}$ (MHz)	Day of occurrence	Magnetic storm phase		
January 16, 2015	BV-5.4	January 07, 2015	-99	BV-13.2	January 08, 2015	Main		
	SLZ-ND			SLZ-ND				
	CXP-6.7			CXP-7.3				
March 10, 2015	BV-4.8	March 17, 2015	-221	BV-7.9	March 18, 2015	Recovery		
	SLZ-6.9			SLZ-9.7	March 17, 2015	Main		
	CXP-6.0			CXP-5.2	March 17, 2015	Main		
April 05, 2015	BV-5.0	April 11, 2015	-75	BV-8.5	April 15, 2015	Recovery		
				-				
				-				
	SLZ-ND			SLZ-ND			-	
May 08, 2015	BV-5.3	May 13, 2015	-76	BV-9.4	May 16, 2015	Recovery		
	SLZ-ND			SLZ-ND			-	
	CXP-ND			CXP-ND			-	
June 05, 2015	BV-5.3	June 23, 2015	-201	BV-10.2	June 25, 2015	Recovery		
	SLZ-5.2			SLZ-11.1			June 23, 2015	Main
	CXP-4.3			CXP-5.0			June 24, 2015	Recovery
July 03, 2015	BV-4.6	July 13, 2015	-61	BV-13.6	July 15, 2015	Recovery		
	SLZ-5.7			SLZ-9.3			July 13, 2015	Main
	CXP-5.9			CXP-8.1			July 14, 2015	Main
August 08, 2015	BV-5.7	August 27, 2015	-92	BV-9.3	August 30, 2015	Recovery		
	SLZ-6.8			SLZ-16.2			August 28, 2015	Main
	CXP-5.7			CXP-11.6			August 27, 2015	Main
October 28, 2015	BV-5.4	October 07, 2015	-124	BV-13.9	October 10, 2015	Recovery		
	SLZ-8.3			SLZ-9.9			October 08, 2015	Main
	CXP-4.8			CXP-4.9			October 08, 2015	Main
December 04, 2015	BV-5.6	December 22, 2015	-155	BV-11.7	December 23, 2015	Recovery		
	SLZ-8.9			SLZ-15.3			December 22, 2015	Main
	CXP - 5.0			CXP-5.3			December 22, 2015	Main
February 25, 2016	BV-5.7	February 03, 2016	-53	BV-14.2	February 04, 2016	Recovery		
	SLZ-8.7			SLZ-15.7			February 04, 2016	Recovery
	CXP-6.0			CXP-11.2			February 03, 2016	Main
February 25, 2016	BV-5.7	February 18, 2016	-57	BV-11.4	February 21, 2016	Recovery		
	SLZ-8.7			SLZ-14.9			February 18, 2016	Main
	CXP-6.0			CXP-6.9			February 20, 2016	Recovery
March 05, 2016	BV-3.4	March 06, 2016	-98	BV-7.9	March 08, 2016	Recovery		
	SLZ-7.4			SLZ-13.2			March 07, 2016	Main
	CXP-5.1			CXP-5.3			March 09, 2016	Recovery

**Table 1**  
Continued

Quiet day	Maximum $f^oE_{s_{quiet}}$ (MHz)	Magnetic storm	Minimum Dst (nT)	Maximum $f^oE_{s_{Dist}}$ (MHz)	Day of occurrence	Magnetic storm phase
August 22, 2016	BV-6.1	August 23, 2016	−74	BV-19.1	August 24, 2016	Recovery
	SLZ-5.1			SLZ-12.1	August 23, 2016	Main
	CXP-6.7			CXP-5.4	August 24, 2016	Recovery
September 13, 2016	BV-5.4	September 01, 2016	−58	BV-12.3	September 03,2016	Recovery
	SLZ-4.5			SLZ-10.1	September 01,2016	Main
	CXP-4.5			CXP-10.4	September 04,2016	Recovery
October 12, 2016	BV-5.4	October 13, 2016	−104	BV-8.7	October 15, 2016	Recovery
	SLZ-8.4			SLZ-9.5/10.3	October 14/15, 2016	Main
	CXP-5.1			CXP-7.1	October 14, 2016	Main
October 12, 2016	BV-5.4	October 29, 2016	−64	BV-14.9	October 30, 2016	Recovery
	SLZ-8.4			SLZ-10.2	October 29, 2016	Main
	CXP-5.1			CXP-8.2	October 30, 2016	Main
May 26, 2017	BV-5.3	May 28, 2017	−125	BV-15.0	May 30, 2017	Recovery
	SLZ-6.6			SLZ-10.1	May 31, 2017	Recovery
	CXP-4.1			CXP-5.1	May 30, 2017	Recovery
July 15, 2017	BV-4.6	July 16, 2017	−72	BV-9.3	July 17, 2017	Recovery
	SLZ-7.4			SLZ-14.1	July 16, 2017	Main
	CXP-5.0			CXP-5.0	July 17, 2017	Recovery
July 12, 2018	BV-5.1	April 20, 2018	−58	BV-13.1	April 21, 2018	Recovery
	SLZ-8.7			SLZ-10.2	April 20, 2018	Main
	CXP-4.5			CXP-5.1	April 20, 2018	Main
May 01, 2018	BV-5.2	May 06, 2018	−56	BV-10.1	May 08, 2018	Recovery
	SLZ-6.8			SLZ-11.3	May 07, 2018	Recovery
	CXP-5.6			CXP-6.8	May 08, 2018	Recovery

Note. ND means that no data is available.

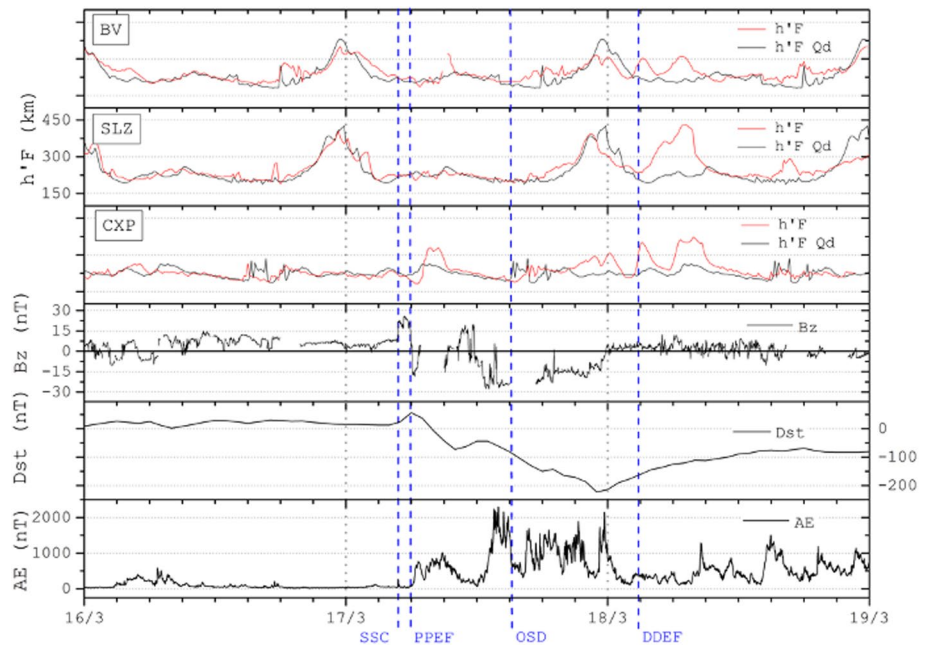
BV, Boa Vista; CXP, Cachoeira Paulista; SLZ, São Luís.

To quantify the magnetic storm effect on the  $E_s$  layer, we calculated the  $f^oE_s$  deviations ( $Df^oE_s$ , in percent) from its quiet time level as follows:

$$Df^oE_s = \left( \left( f^oE_{s_{Dist}} - f^oE_{s_{quiet}} \right) / f^oE_{s_{quiet}} \right) \times 100 (\%), \quad (7)$$

where  $f^oE_{s_{Dist}}$  is the top frequency value for the abnormal  $E_s$  layer during the disturbed day, and  $f^oE_{s_{quiet}}$  is the quiet day value observed at the same local time as the abnormal  $E_s$  layer. Equation 7 is generally used to quantify the positive and negative ionospheric storms in terms of the F2 layer critical frequency and its peak height (Blagoveshchensky & Sergeeva, 2020). The quiet days were selected to be the closest possible to the geomagnetic storms, and they come from the GeoForschungsZentrum Potsdam (<http://wdc.kugi.kyoto-u.ac.jp/qddays/index.html>). Notice that we only considered events in which  $E_s$  layers were observed on both quiet and disturbed days during the same local time. In other words, the  $Df^oE_s$  values are extracted from the difference between the perturbed and quiet days in the  $E_s$  layer observation instant.





**Figure 1.** The disturbed  $h'F$  parameter (red lines) over the three analyzed regions, BV, SLZ, and CXP for the geomagnetic storm from March 16 to 18, 2015. The quiet time values for  $h'F$  (suffix Qd in black line) were manually derived from ionograms considering the diurnal variation on March 10, 2015 for the same regions. The  $B_z$ , Dst and AE indices are presented, respectively, at the three bottom panels.

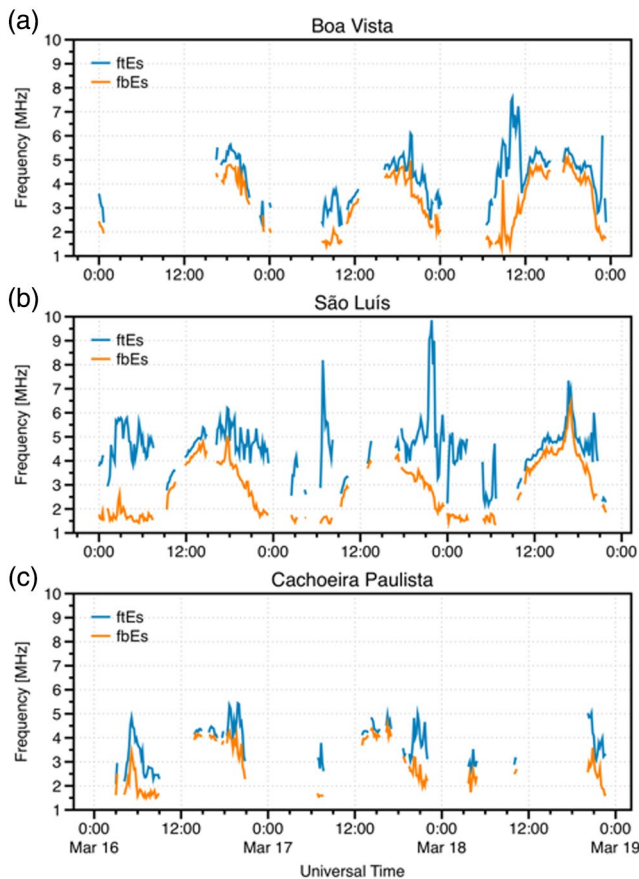
### 3. Results

#### 3.1. The March 17, 2015 Geomagnetic Storm: An Example of a Case Study

The impact of Saint Patrick's magnetic storm in the ionosphere was well studied by several authors (De Michelis et al., 2020; Denardini et al., 2020; Maurya et al., 2018; Tulasi Ram et al., 2019; Spogli et al., 2016; Wu et al., 2016; Zhang et al., 2017). Here, we chose this event as an example of the effects in Es layer dynamics over the Brazilian region during the disturbed periods. Our motivation to study this magnetic storm is that the response of the lower ionospheric parameters is concentrated in the D region (Maurya et al., 2018); TEC distribution (Astafyeva et al., 2015; Spogli et al., 2016; Venkatesh et al., 2017; Wu et al., 2016), F region (Batista et al., 2017; De Michelis et al., 2020; Venkatesh et al., 2017, 2019), and in the space weather indices (Denardini et al., 2020). The St. Patrick's Day storm and its consequences on Es layers were not deeply studied yet as far as we know.

Figure 1 shows the temporal variation of the  $h'F$  parameter (red lines) over the three analyzed regions for the geomagnetic storm that occurred on March 16–18, 2015. Here, we used the  $h'F$  parameter to evaluate the physical mechanism related to the F layer's movement. The reference values (suffix Qd) are superimposed on the respective graphs (black lines), representing the quiet period (the quiet day considered for each geomagnetic storm is placed in the first column of Table 1). The same figure also presents the interplanetary magnetic field  $z$  component (IMF  $B_z$ ), the disturbance storm time (Dst) and the auroral electrojet (AE) indices. All the details about this magnetic storm's interplanetary characteristics can be seen in Yavad et al. (2016).

This magnetic storm was caused by the coronal mass ejection (CME) which arrived in the Earth's magnetosphere on March 17, 2015, causing a Sudden Storm Commencement (SSC) at 0445 UT. The Dst index reached  $-223$  nT at 2200 UT on the same day. Afterward, the recovery phase started. The first southward incursion of the IMF  $B_z$  occurred at around 0600 UT, leading to the beginning of the magnetic storm main phase. After a few reversals the IMF  $B_z$  turned south again at around 1200 UT, maintaining this direction for a longer duration, up to 2300 UT. After that, the IMF  $B_z$  increased, leading to the recovery phase of the magnetic storm. The AE index reached values higher than 2000 nT during the main phase.



**Figure 2.** The *fbEs* (orange line) and *ftEs* (blue line) parameters on March 16–18, 2015, at Brazilian latitudes regions: Boa Vista (a), São Luís (b), and Cachoeira Paulista (c).

In this scenario, we observed two mechanisms acting in the ionosphere: the PPEF (Forbes et al., 1995) and the disturbance dynamo electric field (DDEF) (Blanc & Richmond, 1980). An abrupt increase in the AE parameter together with incursion of the IMF  $B_z$  to negative values was observed on March 17 at around 0600 UT, followed by a decrease in the base height of the layer over the regions, featuring a PPEF (see the line labeled “PPEF” in Figure 1). The PPEF events during this magnetic storm were described by Batista et al. (2017) and Venkatesh et al. (2019). They showed that an eastward PPEF in the afternoon acted as the main driver for the F3 layer formation in the equatorial and low latitudes. Other authors showed that the PPEF caused a strong EIA crest development due to the eastward intense electric field (Astafyeva et al., 2015; Venkatesh et al., 2017).

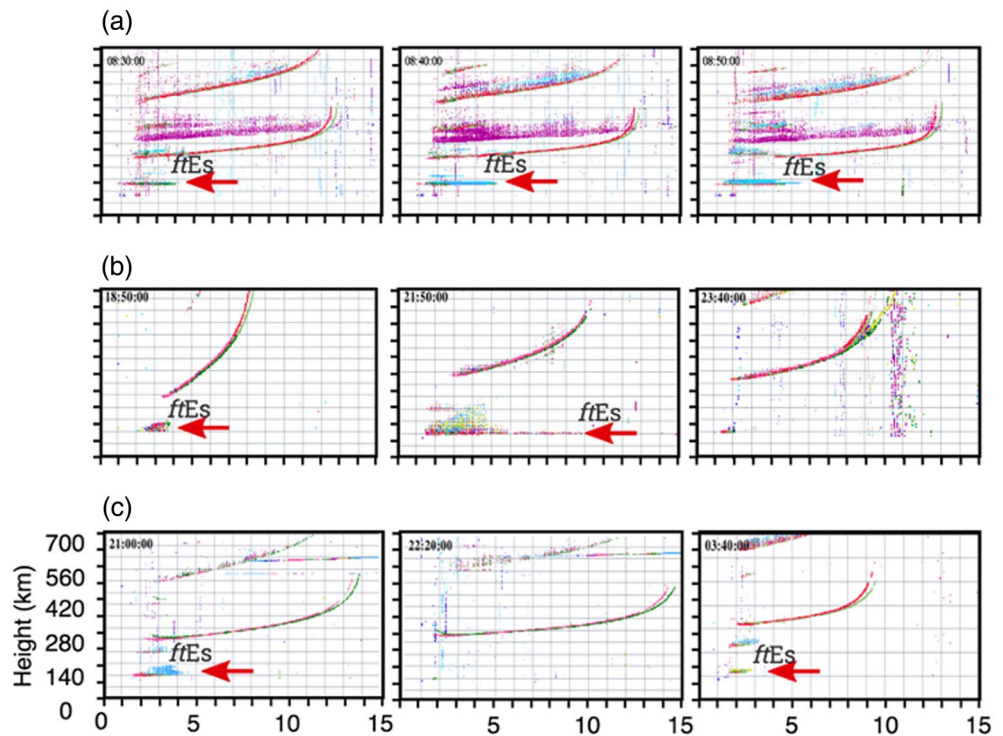
At 1500 UT on March 17, the AE index decreased, indicating the *overshielding* process (see the line labeled “OSD” in Figure 1). At around 2400 UT, the IMF  $B_z$  turned northward. Besides, close to 0300 UT on March 18, the  $h'F$  increased significantly for the three regions. From 0300 UT up to 1000 UT on March 18, the IMF  $B_z$  presented low values prevailing to the northward direction (positive values in Figure 1), and the AE index showed low values, oscillating near 100 nT with an elevation to 1000 nT at around 0900 UT. This behavior provides the appropriate conditions for the disturbance dynamo development. The significant increase of the  $h'F$  parameter at 0300 UT on March 18 confirms that an eastward electric field due to DDEF was present (see, for example, Fejer et al., 1983). The  $h'F$  parameter remains higher than its quiet time value until 1000 UT for the three regions, although for CXP and BV, it shows a tendency of recovery before 0600 UT followed by another increase after that. The double peak observations are out of the scope of the present work. Nevertheless, the main geomagnetic condition and ionospheric electrodynamics are clear indication of the DDEF occurrence, which is the focus of this analysis. At around 2100 UT until the end of the night on March 18, the  $B_z$  oscillated around zero, and the  $h'F$  for equatorial regions (BV and SLZ) decreased compared with the quiet reference day.

The significant modifications in the F region’s electron density distribution over the equatorial and low latitudes were profoundly studied during the Saint Patrick’s magnetic storm event. To analyze the Es layers behavior during this magnetic storm, Figure 2 shows the *fbEs* (orange line) and the *ftEs* (blue line) between March 16 and 18, 2015, for BV (a), SLZ (b), and CXP (c). The typical behavior of the frequency parameters is characterized by enhancement during the morning starting at around 0600 LT, reaching maxima values at around 1200 LT, followed by a steady decrease, reaching the quiescent values after 1800 LT (Resende et al., 2017a; 2017b).

The frequency parameters of the BV region do not reach significant values under normal conditions, mainly during the daytime, because the tidal winds have low amplitudes in this location (Resende et al., 2020). Such behavior is observed on March 16 and 17, when the maximum of *fbEs/ftEs* was 5/6 MHz, and it agrees with the quiet day on March 10 (not shown here). However, at the beginning of March 18, there was a strong enhancement, mainly in the *ftEs* parameter that reached almost 8 MHz. This anomalous Es layer at BV occurred during the recovery phase of this magnetic storm when the DDEF started to be effective.

The Es layer in SLZ suffered a significant enhancement on March 17 during the main phase of the magnetic storm, compared with the previous day (March 16), and quiet period on March 10 (maximum of 8 MHz for *ftEs* as shown in the supplementary material). Although *fbEs* shows a typical behavior, *ftEs* reached frequencies higher than 10 MHz around 2100–2300 UT. Other increases were also observed in the *ftEs* profile. However, this behavior occurred during the daytime and was caused by the strong  $Es_h$  and  $Es_c$  layers occurrences, which are not shown here because it is not the scope of this study. In the nighttime on March 18, the *ftEs* have higher values than the same period of the quiet days.





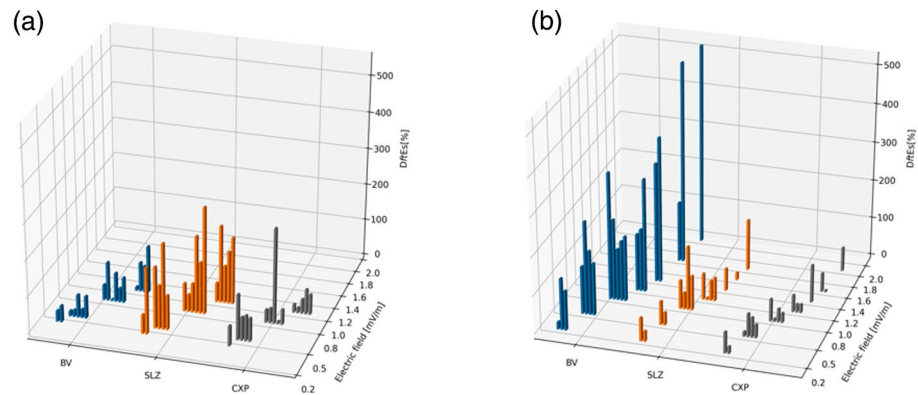
**Figure 3.** Ionograms at (a) Boa Vista collected from 0830 UT to 0850 UT on March 18, 2015, (b) São Luís collected at hours 1850 UT, 2150 UT, and 2340 UT on March 17, 2015, (c) Cachoeira Paulista collected at hours 2100 UT, 2220 UT, and 0340 UT on March 17 and 18, 2015.

On the other hand, the electric fields did not lead to significant modifications in the Es layers over CXP during quiet times (not shown here). In this station, located in a low latitude region, the winds are the primary mechanism responsible for the Es layer formation. They are driven by diurnal, semidiurnal, and terdiurnal tides in the E-region (Mathews, 1998; Pancheva et al. 2003; Resende et al. 2017a; Whitehead, 1961). The Es layer frequency parameters maintained a typical behavior with values below 6 MHz. We also observed the Es layer disruption during a long period between the main and recovery phases of the studied magnetic storm.

Figure 3 shows some selected ionograms for the three regions analyzed. The upper panel (a) represents BV between 0830 UT and 0850 UT on March 18, 2015, showing a strengthening of the Es layers (red arrows). This process started at 0800 UT and lasted up to 1120 UT. This is a blanketing Es layer, classified as “I” type. As mentioned before, the disturbance dynamo process was effective in these hours (Figure 1). Thus, the zonal westward electric field is the most probable mechanism that acted during this atypical Es layer, agreeing with the previous study by Resende et al. (2020).

In SLZ, a strong Es layer appeared at 1900 UT on March 17, 2015. This Es layer reached a maximum frequency equal to almost 10 MHz at 2150 UT. This maximum frequency was determined from the last continuous point of the ionogram signal, as shown by the red arrow in Figure 3b. Afterward, the Es layer weakened and completely disappeared at 2340 UT. It is worth mentioning that two different Es layers seem to be present in hours around 2150 UT over SLZ. We observe an Es<sub>1</sub> layer, and in the background, we note the Es<sub>q</sub> layer occurrence, meaning that the EEJ irregularities can still be effective in SLZ. According to Forbes (1981), a region is generally considered equatorial if the magnetic inclination (dip angle) is up to 7°. Therefore, in 2015, this region was almost in the limit between equatorial and non-equatorial locations (Resende et al., 2016). Thus, the disturbed electric field in SLZ could have influenced the Es<sub>q</sub> layer intensification.

Over CXP we do not observe any expressive Es layer during this period. The ionograms in Figure 3c show a typical Es layer at 2100 UT that disappeared at 2220 UT on March 17, 2015, reappearing around 0340 UT in the next day. This Es layer persists until 0520 UT when it is disrupted again. The Es layer returned to



**Figure 4.** Statistical analysis of the relationship between the Es layer formation and electric field values at BV (blue bars), SLZ (orange bars), and CXP (gray bars) during the (a) main phase and (b) the recovery phase of the magnetic storms. The bars at each station were positioned diagonally to improve the visualization.

normal behavior during the nighttime. It is well-known that the electric field contributions in CXP to the Es layer formation are negligible (Resende et al., 2017a). However, some studies in the literature show that, in particular situations, the Es layer was intensified in this region (Abdu et al., 2014; Batista & Abdu, 1977), because it is under the influence of the SAMA. Thus, other mechanisms can influence the Es layer formation dynamics, such as particle precipitation (Batista & Abdu, 1977), and a significant conductivity enhancement (Abdu et al., 2014). Nevertheless, we did not observe any such behaviors in this case study.

Therefore, it is clear that the Es layer dynamics respond to the magnetic storm effects in different ways, depending on the location under analysis. Thus, we believe that the strong Es layer on BV and SLZ can be influenced by the disturbed electric field, whereas, on CXP, the winds are the principal agent in their formation. This same analysis was applied to the other magnetic storms to improve our understanding of the electric field role in the Es layer formation dynamics for these regions.

### 3.2. Correlation Between Es Layers and Disturbed Electric Fields

We applied the analysis shown in the previous section to the other magnetic storms listed in Table 1. Hence, we observed the Es layer development in the three Brazilian regions during the magnetic storm phases. In this analysis, we computed the drift velocity ( $V_{zE}$ ) using Equation 1 during the nighttime hours to obtain the electric field component using the relationship mentioned in Section 2.2. Given that, we considered the most atypical Es layer occurrence in each storm phase and calculated the deviation  $DfEs$  defined in Equation 7. Thus, we built a relationship between the  $DfEs$  and the electric field values for each station. The results are shown in Figure 4 through the three-dimensional graphs. In this figure, the Es layer statistical analyses at BV (blue bars), SLZ (orange bars), and CXP (gray bars) are presented considering the main phase (Figure 4a) and the recovery phase (Figure 4b) for each one of the magnetic storms analyzed.

It is possible to conclude from Figure 4 that, over the BV station, the electric field influence in the Es layer during the main phase is weak compared with the recovery phase. In the former, the Es layer strength did not show strong variation with the electric field, whereas, in the later, the Es layers intensified for higher electric fields. Furthermore, the Es layers in BV during the recovery phase were significantly stronger than those of the main phase, with a density increase from 90% up to 500%.

In SLZ, we observe an inverse behavior because the Es layers were almost 90% stronger in the main phase compared to the quiet times. This occurred for the electric field values ranging from 0.5 to 1.4 mV/m. In this region, it is not possible to infer any correlation between the electric field intensity and the Es layer density during both phases.

Over the CXP region, only one case showed a significant density increase (97%) in relation to the quiet period which occurred during the main phase. Furthermore, it is also not possible to observe a clear correlation between the electric field intensity and the Es layer density during both phases of the magnetic storm.

To provide a broader view of the relationship between the Es layer development and electric field values, Table 2 presents the  $fE_s$  variation concerning the quiet reference day (Equation 7) as well as the respective electric field at each magnetic storm phase. It is important to mention that the electric field calculated for the equatorial station SLZ was used for all the regions analyzed since the electric field can be mapped from the equatorial F region to low latitudes through the magnetic field lines (Abdu et al., 2014). Furthermore, the locations of the regions in this study have similar longitudes. Thus, the longitudinal variation does not cause a significant influence on the electric field values.

We calculated the vertical drift velocity around the atypical Es layer occurrence hours. This drift is then used to obtain the zonal electric field (Abdu et al., 2005; Kelley, 1989) from the drift equation  $V = E \times B / B^2$ , in which the International Geomagnetic Reference Field provides the magnetic field  $B$ . This relationship concludes that a 1 mV/m zonal electric field produces a vertical drift of 40 m/s. In this analysis, the maximum computed drift velocity was considered when obtaining the electric field. Notice that we do not estimate the other electric field components because they do not significantly influence the Es layer dynamics over the analyzed regions (Abdu et al., 2014; Resende et al., 2020).

As mentioned before, the Es layers in CXP had almost no significant changes when the two magnetic storm phases are compared. At low latitudes, the wind shear mechanism is predominant, and therefore, the electric field plays only a secondary role in the Es layer formation (Haldoupis, 2011; Haldoupis et al. 2006; Whitehead, 1961). Prasad et al. (2012) studied the Es layer behavior in different regions of the globe, and they concluded that the magnetic storm effect in the Es layer at middle latitudes is very weak, considering it negligible. During disturbed times, the only mechanism that modifies the Es layers over the CXP region is the particle precipitation. As mentioned earlier, the effectiveness of this mechanism is verified through the  $E_s^a$  layers, shown in Batista and Abdu (1977). However, the  $E_s^a$  was not observed in our data. Therefore, we believe that this mechanism did not act in the period studied despite the intense geomagnetic storm.

Over SLZ, a region close to the magnetic equator, our results pointed out that the disturbed zonal electric field can cause modifications in the Es layer formation, mainly during the magnetic storm main phase. However, this behavior does not follow a specific pattern. It is important to mention here that the geomagnetic field inclination in the Brazilian sector varies at a rate of 20' per year, corresponding to an apparent northwestward movement of the magnetic equator (Batista et al., 2011). Thus, the SLZ site is not considered an equatorial station nowadays since the magnetic equator is departing from this region. Although the wind shear mechanism is efficient at the SLZ region, forming blanketing layers, we also observe the  $E_s^q$  and other Es layer types in these disturbed periods. It means that the electric field of the EEJ instabilities could still work together with the tidal winds in the Es layer formation process. Depending on the electric field direction, the EEJ plasma irregularities could be stronger, leading to higher  $fE_s$  (Resende & Denardini, 2012; Resende et al., 2013). This fact explains some Es layers being strengthened in some cases during the main phase of the magnetic storms in SLZ.

The strong Es layers that occurred in BV confirm the hypothesis in Resende et al. (2020), in which the most probable mechanism acting during these atypical Es layers was the zonal westward electric field caused by a disturbance dynamo. The authors did a deep case study using observational data and simulations to show some evidence that the Es layer density is significantly enhanced when the disturbed zonal electric field is present. However, they affirmed that the electric field effect in the Es layer formation over BV still needed more in-depth analysis. In the present work, the strong Es layer in BV was observed in all events during the analyzed magnetic storm recovery phases. In the following sections, we discuss the physics of these Es layers in BV to show their relationship with the DDEF.

Lastly, the electric field value presented in Table 2 varies between 0.2 and 2 mV/m, agreeing with the intensity of the disturbed electric that penetrates to the ionosphere (Gonzalez et al., 1994; Tsurutani et al., 2008). As we did not find in the literature a quantitative electric field effect on the Es layer formation, we provide this analysis as follows.

### 3.3. The Threshold Value of the Electric Field in the Es Layer Formation

The MIRE model has been used to simulate the Es layers with a high confidence level over the Brazilian sector (Moro et al., 2017; Resende et al., 2017a, 2017b, 2016; Resende et al., 2020). At low latitudes, the electric

**Table 2**  
*The Magnetic Storm Events Used in This Analysis, the Electric Field Value, and the Percentage Variation of the DftEs Parameter for Each Magnetic Storm Phase in BV, SLZ, and CXP.*

Event	Electric field		DftEs (%)	
	Main phase (mV/m)	Main phase	Recovery Phase (mV/m)	Recovery phase
January 07, 2015	0.4	BV-29	2	BV-517
		SLZ-No Data		SLZ-No Data
		CXP-2		CXP-61
March 17, 2015	1	BV-27	1	BV-162
		SLZ-51		SLZ-51
		CXP-21		CXP-20
April 11, 2015	0.5	BV-1	0.5	BV-166
		SLZ-No Data		SLZ-No Data
		CXP-No Data		CXP-No Data
May 13, 2015	-	BV-No Data	0.8	BV-155
		SLZ-No Data		SLZ-No Data
		CXP-No Data		CXP-No Data
June 23, 2015	0.5	BV-17	0.2	BV-18
		SLZ-168		SLZ-60
		CXP-89		CXP-54
July 13, 2015	0.1	BV-5	0.2	BV-241
		SLZ-2		SLZ-21
		CXP-1		CXP-1
August 27, 2015	0.5	BV-44	1.5	BV-155
		SLZ-183		SLZ-132
		CXP-54		CXP-47
October 07, 2015	1	BV-9	1	BV-294
		SLZ-211		SLZ-5
		CXP-13		CXP-21
December 22, 2015	0.8	BV-41	1	BV-148
		SLZ-76		SLZ-67
		CXP-39		CXP-43
February 03, 2016	0.8	BV-123	0.8	BV-200
		SLZ-9		SLZ-78
		CXP-11		CXP-20
February 18, 2016	1	BV-79	1	BV-79
		SLZ-101		SLZ-101
		CXP-38		CXP-38
March 06, 2016	0.8	BV-20	1.5	BV-520
		SLZ-78		SLZ-18
		CXP-20		CXP-3
August 23, 2016	0.8	BV-78	0.5	BV-209
		SLZ-211		SLZ-145
		CXP-25		CXP-60

**Table 2**  
*Continued*

Event	Electric field	DftEs (%)	Electric field	DftEs (%)
	Main phase (mV/m)	Main phase	Recovery Phase (mV/m)	Recovery phase
September 01, 2016	0.8	BV-37	0.2	BV-102
		SLZ-140		SLZ-26
		CXP-6		CXP-34
October 13, 2016	0.5	BV-61	1	BV-169
		SLZ-118		SLZ-89
		CXP-63		CXP-24
October 29, 2016	0.8	BV-10	0.5	BV-377
		SLZ-293		SLZ-32
		CXP-40		CXP-17
May 28, 2017	1	BV-70	0.8	BV-309
		SLZ-142		SLZ-165
		CXP-67		CXP-34
July 16, 2017	1	BV-127	0.5	BV-272
		SLZ-183		SLZ-4
		CXP-54		CXP-6
April 20, 2018	0.5	BV-22	0.8	BV-133
		SLZ-235		SLZ-60
		CXP-69		CXP-51
May 06, 2018	0.5	BV-60	0.8	BV-135
		SLZ-94		SLZ-57
		CXP-63		CXP-97

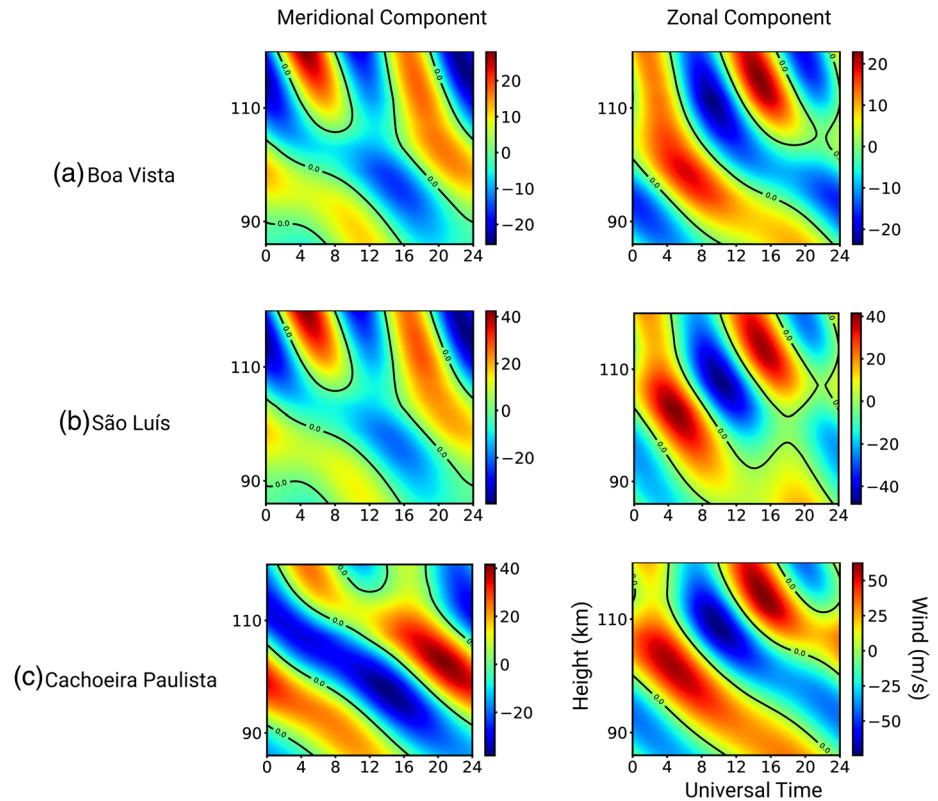
Abbreviations: BV, Boa Vista; CXP, Cachoeira Paulista; Dst, disturbance storm time; SLZ, São Luís.

field was neglected without affecting the simulation accuracy (Resende et al., 2017a; 2017b). For regions around the magnetic equator, the electric field of the EEJ current was used to study the Es layer development (Moro et al., 2017; Resende et al., 2016). Recently, using the MIRE simulations, Resende et al. (2020) showed a possible connection between the westward electric field and the strong Es layer that occurred in the geographic equator region.

In the present work, based on the electric field values derived from drift velocity (Table 2), we analyzed their influence at each region considered in this study. First, we fitted the wind profile for the three stations using the GSWM-00. This process is required to obtain values that represent better the Es layer dynamics. We used 80% of the wind amplitudes for São Luís and 90% of the amplitudes for Cachoeira Paulista, which best resolve the Es layer formation in our simulations. Figure 5 shows the wind amplitudes (color scale) computed using the wind parameters in Equations 5 and 6. The map format in this figure given in height versus universal time (UT) refers to the diurnal and semidiurnal tidal wind for the meridional and zonal components over BV (a), SLZ (b), and CXP (c). The wind parameters for March were used to generate the maps. Although the tidal winds have a seasonal variation, the purpose of this work is to verify the electric field effect. Thus, the GSWM-00 model's amplitudes are satisfactory to be used as a background profile for this purpose. Finally, notice the presence of wind shearing in all components (zeros in the profile), which is a necessary condition to produce Es layers.

The results in Figure 5 show that the wind amplitudes are much lower over the BV region than at SLZ and CXP stations. This behavior corroborates with the fact that weak Es layers are seen in the observational data at BV. In this station, we observed that the meridional wind amplitude is almost equal to the zonal amplitude, with values around 30 m/s. SLZ and CXP present the most intense wind profiles. In general, the wind

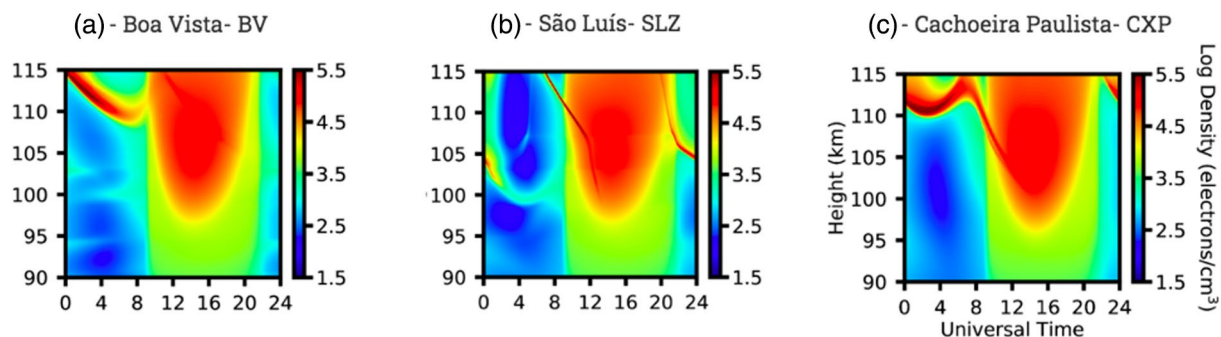




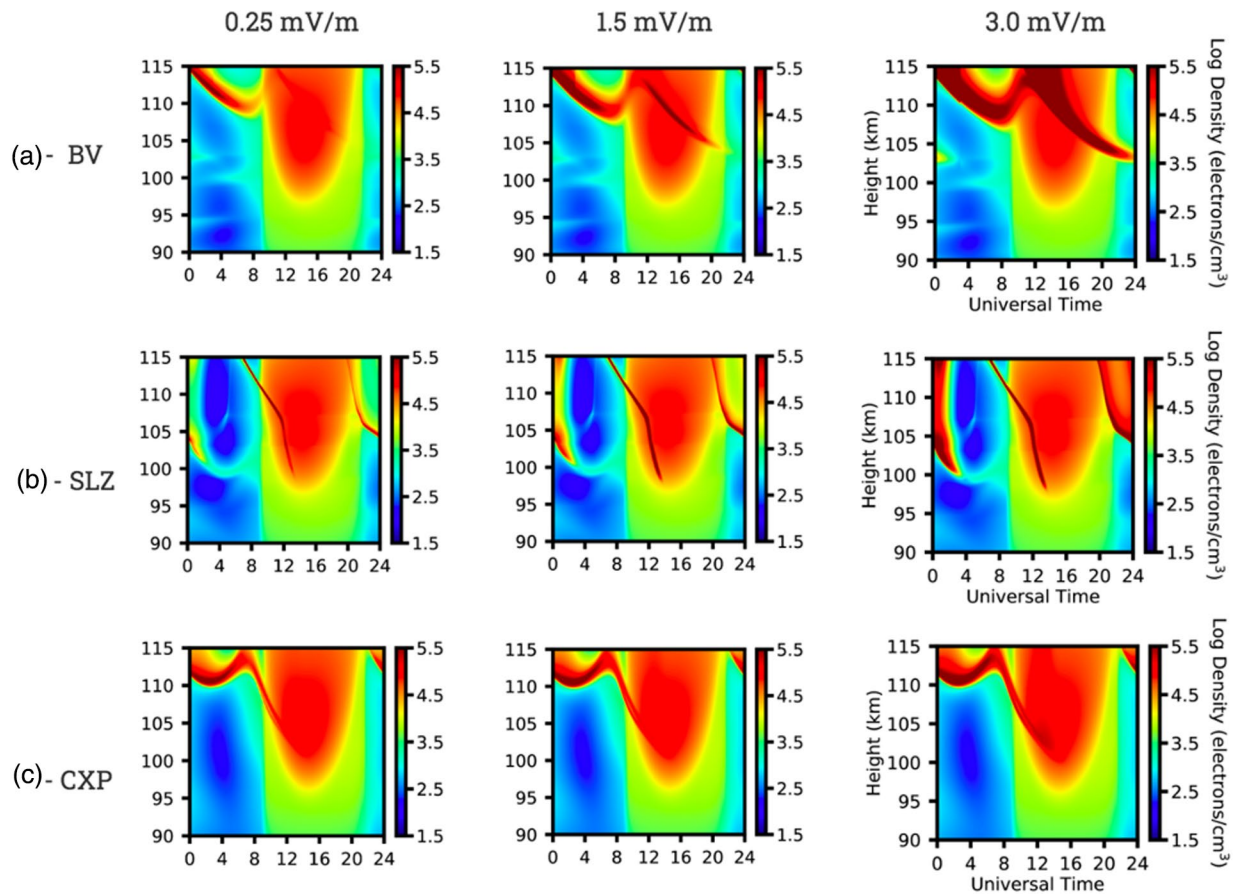
**Figure 5.** Wind profile of the meridional and zonal components obtained using GSWM that was included in MIRE to simulate the Es layers over BV (a), SLZ (b), and CXP (c) in March 2015.

behavior over SLZ and CXP agrees with the previous analysis in Resende et al. (2017a, 2017b), in which they used data from a meteor radar to obtain the wind components. In this work, we chose the GSWM-00 model since it yields good results for our interest zone, which is around 100–110 km. We also observed that the wind behavior is similar over BV and SLZ, which is expected since we are considering the equinoctial condition, and the distances of those regions to the geographic equator are almost the same.

Figure 6 shows the results of the simulations considering only the tidal winds profile shown in Figure 5 over (a) BV, (b) SLZ, and (c) CXP. In these figures, the electron density (log scale) is plotted as a function of time (in UT) and height (Height-Time-Intensity, HTI maps). Here, we considered the height up to 115 km, which encompasses the range of our interest. As discussed in Resende et al. (2017a), MIRE successfully simulated the E region electron density with low values in the night and expressive electron density in the daytime. Also, the thin layers of enhanced electron density seen in the HTI maps are the Es layers. These Es layers



**Figure 6.** Electron density as a function of Universal Time (UT) and height (km) simulated by MIRE considering the diurnal and semidiurnal tidal winds in (a) BV, (b) SLZ, and (c) CXP on March 2015.



**Figure 7.** Electron density simulated by MIRE considering the winds and distinct values of the zonal electric field (0.25 mV/m, 1.5 mV/m, and 3.0 mV/m) in (a) BV, (b) SLZ, and (c) CXP.

simulated performed a downward movement, which is the typical behavior of their electrodynamics (Hal-doupis et al., 2011). This behavior occurs due to the semidiurnal and diurnal periodicity that characterizes the Es layer movement (Resende et al., 2017a).

During the daytime, the electron density of Es layers in BV is very close to the E region peak density. This behavior occurs due to the low wind amplitudes around the geographic equator regions, as mentioned before. These Es layers are more expressive during the nighttime, agreeing with what we have seen in observational data. Over SLZ, the Es layer is denser in the daytime than in the night hours. In CXP, the Es layers occur during all day, with similar density. We also noticed that the simulated Es layers are in high altitudes in some hours with an evident downward movement. This fact reinforces that the winds play a fundamental role in the Es layer formation over these regions.

To analyze the electric field effect in the Es layer development, we performed multiple simulation scenarios considering a constant westward zonal electric field with values ranging from 0.25 mV/m to 3.0 mV/m and a step of 0.25 mV/m. This analysis aims to estimate the Es layer fraction that strengthens due to the electric field value. The simulations indicated that there are different threshold values for each region. To exemplify some results, we show the HTI maps in Figure 7 for (a) BV, (b) SLZ, and (c) CXP. In this figure, we present the evolution of the electron density taking into account the tidal winds and the minimum, intermediate, and maximum values of the electric field zonal component used in this study.

Comparing these results with the previous one, which considers only tidal winds (Figure 6), it is noted that the Es layer electron density increases as the electric field component increases. In BV, the simulated thin layers that characterize the Es layer are not forming with 3.0 mV/m. On the other hand, for the same electric field value, a denser and thin Es layer is observed during the daytime in SLZ. This result shows that

**Table 3**  
*Maximum Intensity in the Es Layer Occurrence Observed in Simulation for Each Electric Field Value Tested in MIRE, as Well as the Percentage of the Es Layer Increases Concerning the Same Hour of the Simulations That Consider Only the Wind Profiles.*

Electric field (mV/m)	Maximum value of electron density in simulations (log density)	Increase (%)
0.00	BV-5.50	–
	SLZ-6.21	–
	CXP-5.53	–
0.25	BV-5.65	30.8
	SLZ-6.46	48.3
	CXP-5.56	5.5
0.5	BV-5.76	58.7
	SLZ-6.84	162.8
	CXP-5.59	11.3
0.75	BV-5.87	91.7
	SLZ-6.98	221.8
	CXP-5.62	17.5
1.0	BV-5.98	130.8
	SLZ-7.41	485.1
	CXP-5.62	17.5
1.25	BV-6.09	177.0
	SLZ-7.63	684.0
	CXP-5.68	30.6
1.5	BV-6.21	236.7
	SLZ-7.81	889.9
	CXP-5.71	37.7
1.75	BV-6.32	301.3
	SLZ-7.95	1082.3
	CXP-5.74	45.1
2.0	BV-6.43	376.9
	SLZ-8.07	1273.4
	CXP-5.78	55.6

BV, Boa Vista; CXP, Cachoeira Paulista; SLZ, São Luís.

although the wind profiles were symmetric, the electric field influence is different in these regions. Also, in CXP, the electric field does not seem to have an immediate influence as observed over BV, in which the electron density of the Es layers intensifies gradually. The main difference in simulations is that the electric field variation does not cause a significant modification in the Es layer process in CXP, as shown in the results for 0.25 mV/m (density increase of ~6%) and 1.5 mV/m (density increase of ~38%). However, the same variation causes a significant strengthening of the Es layer in simulations over BV and SLZ, reaching a density increase of ~236% and ~890%, respectively for an electric field of 1.5 mV/m.

To further support our claim that the electric field is the main responsible for the Es layer strengthening in regions near the equator, Table 3 shows the maximum intensity in the Es layer occurrence for each electric field value tested in MIRE. Additionally, we show the percentage of the Es layer increases concerning the same hour of the simulations that consider only the wind profiles. It is essential to mention here that the Es layer's maximum density occurred around 0300 UT, 0500 UT, and 0400 UT for BV, SLZ, and CXP, respectively.

In Figure 7 we observe a significant intensification during the nighttime in SLZ. The Es layer increase in simulations can be greater than 1000%, which does not agree with the observational data shown in Figure 4. Electric field values up to 0.75 mV/m in the model simulate Es layers that show good correlation with the observational data. For higher electric field values the simulation results were unrealistic. Thus, the threshold (limit) value of the electric field to form the Es layer for this region is 0.75 mV/m during the disturbed period. We believe that the unsatisfactory results in this region can be due to other Es layer formation mechanisms not included in MIRE, such as EEJ instabilities. We will discuss this behavior in more detail in the next section.

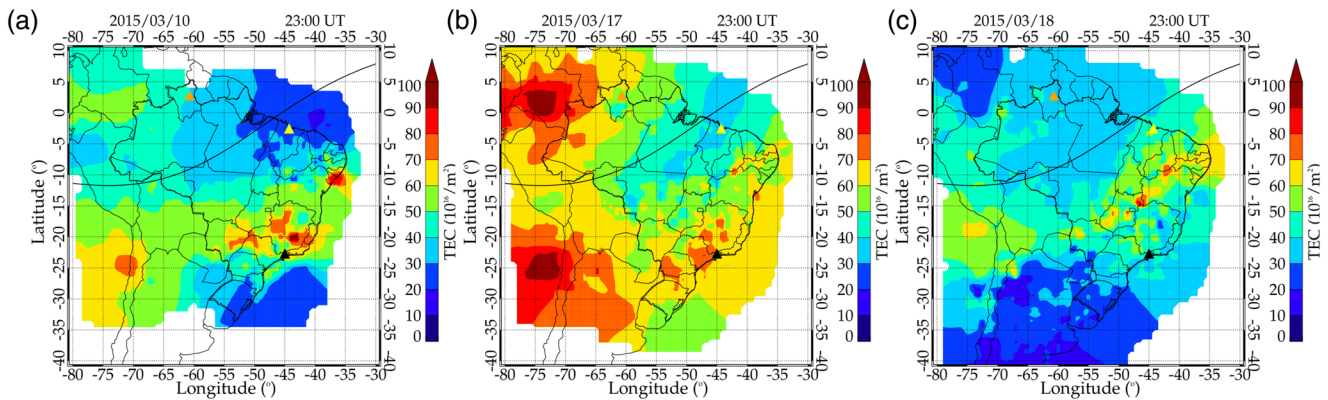
Over BV, the intensification values in simulations have a reasonable correlation with the observational data, showing that the model reacts well to the wind and electric field behavior in this region. We notice that the threshold electric field value to form the Es layer in BV is 2.5 mV/m, that is when the model still converges, and the electron density is satisfactory compared with the observational data for the Es layer reported in the literature (Resende et al., 2017a; 2017b; Resende et al., 2020). The Es layer becomes extensive with unrealistic values when the electric field is equal to 3 mV/m, as shown in Figure 7.

Finally, the electric field variation causes low modification in the Es layer formation in CXP, showing that tidal winds are dominant over this station. The Es layer increased by a maximum of 55% in simulations, while

the observational data show intensifications around 60% in most cases of this analysis. The model was able to simulate the Es layers for electric field values up to 3.7 mV/m, but the electron density did not continue to increase significantly. Therefore, in the next section, we try to discuss the competing roles of electrodynamic and dynamical processes in the Es layer formation over these three regions studied.

#### 4. Discussions

In this work, we evaluate the electric field effect in the strengthening of the Es layer over the Brazilian sector. The results have shown that the electric field is effective in the Es layer formation during the recovery phase of magnetic storms in BV and during the main phase of magnetic storms in SLZ. Nevertheless, over the CXP region the electric field does not seem to cause a significant influence in the Es layer formation.



**Figure 8.** Longitude versus latitude distribution of the TEC map over South America at 23 UT before and during the Saint Patrick's magnetic storm for (a) a quiet period, (b) the day when the PPEF is effective, and (c) the day when the DDEF effect is acting. The black line refers to the geomagnetic equator, and the triangles are BV (orange), SLZ (yellow), and CXP (black) regions. The color scale indicates the TEC intensity.

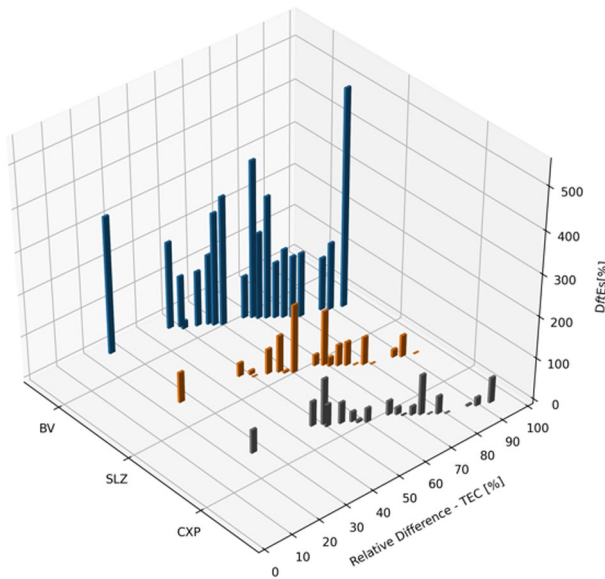
Therefore, to investigate which phenomenon occurs in areas around the equatorial/magnetic equator, we used also additional techniques to those shown in previous sections. First, we emphasize here that the wind shear mechanism is the main driver for the Es layer formation over the Brazilian sector. We believe that during the disturbed periods, the electric field is superposed to tidal winds reinforcing the Es layers.

In relation to the BV region, Resende et al. (2020) showed that DDEF is a possible mechanism to trigger the atypical layers in this region. They observed three cases that the DDEF leads the observed Es layer strengthening. However, they affirm that further study would be required to compute the statistical behavior of such occurrences. As described in Resende et al. (2020), to analyze the electric field performance, we processed the vertical drift during our interest hours, that is when the atypical Es layer occurs. The positive drift values mean that the electric field points eastward, whereas negative drift values indicate that it points westward. Here, we found westward electric fields during all the cases under analysis.

Therefore, to confirm that the DDEF is acting, we used the total electron content (TEC) to analyze the weakening of the equatorial ionization anomaly (EIA) in some hours, which indicates the DDEF occurrence. Therefore, maps of the South America TEC were analyzed. The TEC is calculated using a technique developed by Otsuka et al. (2002), in which a weighted least squares fitting determines the instrumental biases, assuming that the hourly TEC average is uniform. The maps show the TEC in a two-dimensional form, and they are available in Brazilian Studies and Monitoring of Space Weather (Embrace - <http://www2.inpe.br/climaespacial/portal/en/>). These TEC maps have a 10 min time resolution and  $0.5 \times 0.5^\circ$  of spatial resolution in latitude and longitude. More details about the TEC maps methodology can be found in Takahashi et al. (2014, 2016).

The quiet time behavior of the TEC in the maps shows a high-density observation area extending between  $20^\circ$ – $30^\circ$ S and  $40^\circ$ – $60^\circ$ W, which characterizes the EIA. This anomaly occurs due to the fountain effect in which the plasma along the geomagnetic equator is raised under the action of the EXB drift and subsequently it moves downwards along magnetic field lines, under the action of diffusion and gravity, generating plasma crests over the off-equatorial region, in the Northern and Southern Hemispheres. Generally, the EIA is well developed at 2300 UT (19–20 LT in Brazilian longitudes) and its peaks can be observed around  $\pm 15^\circ$  magnetic latitude in TEC maps. Figure 8 shows the TEC maps over South America during the days around the St. Patrick magnetic storm that is used as an example in our analysis. The TEC map during the reference quiet day (March 10, 2015) at 2300 UT is presented in Figure 8a, whereas Figures 8b and 8c represent the disturbed days, March 17 and 18, 2015, respectively at 2300 UT. The geomagnetic equator is given in the black line, and the triangles refer to the BV (orange), SLZ (yellow), and CXP (black) regions. It is possible to notice an enhancement in TEC at the EIA crests on March 17, 2015, confirming that an eastward PPEFs is acting, as already shown in Figure 1. On March 18, 2015, we observed an apparent weakening of the EIA crest near sunset time compared with the typical behavior of the ionosphere plasma over Brazil (Figure 8a). Hence, the EIA's weakening shows that the zonal westward electric field caused by a DDEF is





**Figure 9.** Statistical analysis of the relationship between the strong *Es* layer formation and EIA weakening during the recovery phase of magnetic storms. The bars at each station were positioned diagonally to improve the visualization.

present. Although the DDEF started from 0300 UT (Figure 1), the TEC maps suggest that it lasted until ~15 h later. The high values of *f*<sub>TE</sub>s that also occurred in the nighttime period on March 18, 2015 (see Figure 2a), support this statement in BV.

To see the DDEF effect and the connection with the strong *Es* layers in all magnetic storms used in this study, we analyze the relative difference (RD) parameter over the TEC maps. The RD (Equation 8) is calculated through the TEC maps for each day that we observe the strong *Es* layers ( $TEC_{Dist}$ ) concerning the typical (non-disturbed) day ( $TEC_{Ref}$ ) of each magnetic storm used in this analysis given in Table 1. We used the EIA peak between 20° and 30°S at 2300 UT to perform this analysis, selecting the highest RD value in this latitude range. RD is computed here as follows:

$$RD (\%) = \left( \left( \frac{TEC_{Ref} - TEC_{Dist}}{TEC_{Ref}} \right) \right) \times 100. \quad (8)$$

Thus, we correlated the *Df*<sub>TE</sub>s during the recovery phase of the magnetic storms with the RD parameter. Here, we used as a  $TEC_{Dist}$  reference, the day that the strong *Es* layer occurred in BV. Figure 9 shows a 3D graph distribution for each station in this analysis at BV (blue bars), SLZ (orange bars), and CXP (gray bars). In the most extreme case, the *Es* layer density increased more than 500% in BV, whereas the EIA weakened almost 100%, i.e.,  $TEC_{Dist} \approx 0$ . Therefore, this analysis indicates that DDEF action is a significant factor in the anomalous *Es* layer formation in BV,

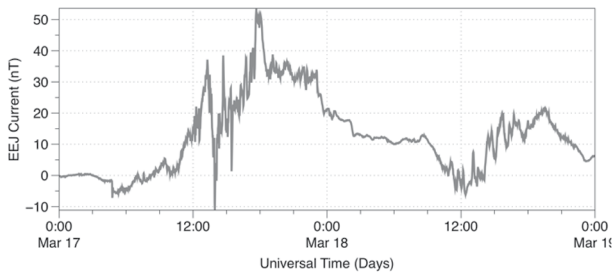
confirming the assumption in Resende et al. (2020). This correlation is important since the presence of a strong *Es* layer in the ionograms at BV can be an indicator of the DDEF when the TEC data are not available.

During the magnetic storm recovery phases, the electric fields do not have a significant effect in SLZ and CXP. Therefore, we observed a low correlation between the EIA weakness (due DDEF effect) and the *Es* layer formation in these regions. We believe that the DDEF does not cause notable influences in SLZ or CXP because other mechanisms act together in the *Es* layer formation in these regions. These *Es* layer modifications may even be due to the seasonal wind variation, mainly in CXP (Resende et al., 2017a). One crucial factor is that the tidal wind amplitudes are higher in SLZ and CXP than in BV, showing that the wind shear mechanism can give rise to the denser *Es* layers in such regions.

The *Es* layers reached high frequencies in some cases over SLZ during the main phase of the magnetic storms, as shown in Figure 4. A study performed by Rastogi et al. (2012) related the *Es* layer modifications with the *undershielding/overshielding* electric fields over the equatorial and low latitude regions. They observed that these layers occurred during the main phase of magnetic storms in the equatorial region and are associated with the large westward PPEF. Additionally, Abdu et al. (2014) affirm that the zonal westward electric field during disturbed times (*overshielding*) contributes to the formation of the *Es* layer around equatorial/low latitudes. They attributed these anomalous *Es* layers to the enhanced ratio of the field line integrated Hall to Pedersen conductivity ( $\Sigma_H/\Sigma_P$ ), which is possible due to the SAMA presence. However, in the main phase of the Saint Patrick's magnetic storm, TEC data showed an intensification of the EIA, representing an *undershielding* process (eastward electric field) during the daytime, and it is expected that the *Es* layer disappears (Abdu et al., 2014). Thus, we believe that the electric field effect in SLZ indicates that other mechanisms could be acting. This fact corroborates with the irregular pattern of the strong *Es* layers in this station, observed through the low correlation between the electric field intensity and the *Es* layer density in the statistical study. Furthermore, we do not find any evidence of particle precipitation over SLZ and CXP, thereby discarding the SAMA influence.

In our study, some ionograms in SLZ caught our attention. One example is the *Es* intensification in SLZ during the main phase of the St. Patrick magnetic storm (Figure 3b). In this case, it is evident that the *Es* layers are blanketing layers ("f" type), but it also seems to have an irregularity layer (*Es<sub>q</sub>* layer) in the background.





**Figure 10.** Temporal evolution of the EEJ ground strength on March 17–18, 2015, using the magnetometer data from two sites: SLZ (equatorial station) and EUS (off equatorial station).

Here, we strongly believe that the  $Es_q$  layer occurs because of the high frequency that this layer reached ( $fEs > 9$  MHz) since the tidal wind behavior is not so strong in this region, as mentioned in Resende et al. (2017b). Also, at the same time, the  $Es$  layers blocked the upper regions meaning that the  $Es_y$  is present. Therefore, we conclude that 2  $Es$  layers were present on the same day, and the SLZ location might still be under some influence of the EEJ current. This result closely resembles those obtained by Devasia et al. (2006), in which they studied the characteristics of different  $Es$  layer types and their association with the plasma density irregularities over the magnetic equator. The authors concluded that the Gradient Drift instability structures may occur when the EEJ current is not strong. In such cases, the  $Es_q$  layers can be formed simultaneously with other  $Es$  layer types. Thus, we believe that, in the analyzed case, an electric field imposed during the magnetic storm main phase may have contributed

to form the Gradient Drift instability. In turn, this mechanism produced the  $Es_q$  layer, even if the studied station is located in the magnetic equator border.

To corroborate our hypothesis that there is more than one mechanism acting in the  $Es$  layer formation in SLZ, we evaluated the magnetometer data for the St. Patrick magnetic storm event. Figure 10 shows the EEJ ground-strength variation as a function of UT for the disturbed periods analyzed (March 17 and 18, 2015). The magnetic data treatment consists of analyzing the five quietest days in a respective month and obtaining the average local midnight values. Thus, this average is subtracted from each value of the  $H$  component, providing the  $\Delta H$  for the corresponding station. To evaluate the EEJ current, we used data from an equatorial station SLZ, and from an off-equatorial station, Eusébio (EUS, 03.89°S, 38.44°W, dip:  $-14.83$ ). Thus, the variation of the EEJ ground strength is estimated by taking the difference between the  $\Delta H$  values of these stations ( $\Delta H_{SLZ} - \Delta H_{EUS}$ ). A more detailed explanation of the magnetic data treatment and the use of the two stations can be found in Denardini et al. (2009).

Two important characteristics were observed in Figure 10 on March 17, 2015, such as (i) there is a period of reversed electrojet currents (CEJ events) during the daytime that coincides with the absence of  $Es$  layer (around 13–16 UT in Figure 2), and (ii) the EEJ current is intensified during the same time that the strong  $Es$  layer occurs in SLZ (around 20–23 UT in Figure 2). These characteristics are a real manifestation of the Gradient Drift instability, which is driven by the vertical polarization Hall electric field and the density gradient causing diffuse traces in ionograms, the  $Es_q$  layers. It is important to mention here that the eastward electric field intensifies these irregularities. Thus, the unrealistic results of MIRE model probably occur because the Gradient Drift instability is not considered in the simulations, as seen in Resende et al. (2016) and Moro et al. (2017). In fact, in transition regions such as SLZ, under the limiting modification of influence of the EEJ, the competing roles of electrodynamical and neutral-dynamical processes (wind shears) in the  $Es$  layer formation are frequent, and we observed different types of  $Es$  layers in ionograms (Resende et al., 2016). Thus, we have here evidence that there is a possibility that the EEJ current still causes irregularities over the SLZ station.

The above affirmation is supported in some previous works. The regions are considered an equatorial station until a magnetic inclination of  $7^\circ$  (Forbes, 1981), and consequently, the  $Es_q$  layers occurred in such areas. However, Moro et al. (2016) showed that the vertical electric field of the EEJ current, responsible for the Gradient Drift instability occurrence, is strong around 100 km in recent years in SLZ ( $I \geq 7^\circ$ ), where  $Es_q$  usually appears. Furthermore, Resende et al. (2016) showed that in 2015, in which the magnetic inclination in SLZ was around  $7.8^\circ$ , the  $Es_q$  layers still occurred during a few hours. The authors also showed that during the disturbed periods in the daytime, the weakness/disruption of this  $Es$  layer type is frequent due to the CEJ events (Denardini et al., 2016; Resende & Denardini, 2012; Resende et al., 2013). The  $Es_q$  layers only returned when the EEJ would establish for its typical conditions, eastward (positive) at daytime. This behavior seems to have occurred in our analysis, as seen in the correlation between Figures 2 and 10. The  $Es_q$  and the  $Es_b$  layer occurrences show that the strengthening  $Es$  layer during the main phase in some cases is due to the EEJ electric field that operates in increasing instabilities in this region. Thus, it is not a rule that the disturbed electric field and winds can cause an intense  $Es$  layer over SLZ as at the BV region.

Additionally, as mentioned before, we believe that the model used here does not show satisfactory results when the electric field is included in SLZ because different mechanisms acted in the Es layer development in this region. In other words, we credit these discrepancies in our simulations because we do not consider the EEJ dynamics in MIRE.

Also, our results over CXP agree with the recent analysis performed by Conceição-Santos et al. (2019), in which they analyzed the different types of Es layer during four months in São José dos Campos (23.2°S, 45.8°W, dip: ~21.0°), a station near to CXP. They did not observe the  $Es_a$  layers, indicating the absence of the particle precipitation mechanism, as mentioned before. Nevertheless, they found one case in which a moderate increase occurred in the Es layer frequencies during the disturbed period of 01–05 September 2016. In this magnetic storm, the Es layer density in CXP increased by 34% in the main phase, as shown in Table 2. Conceição-Santos et al. (2019) suggested that the Es electron density enhancements are associated with redistribution of ionization driven by the wind shear mechanism. Thus, we believe that the only effective mechanism in the Es layer development during these years is the tidal winds. Therefore, the variations concerning the quiet periods in CXP can be associated with the seasonal tidal wind variabilities, as shown in Resende et al. (2017a).

Finally, it is remarkable that the electric field influence in the strong Es layers is specific of the regions near the geographic equator. Our analysis corroborates with the proposal of Resende et al. (2020), in which the intensifications observed in BV are associated with DDEF. The low amplitudes of the winds over the BV station seem to favor the electric field influences in the Es layer modifications. Furthermore, in SLZ, we notice some irregular intensifications that occurred during the magnetic storm's main phase. Our results give an indication that the EEJ instabilities might still be present over the SLZ station. Over CXP, the tidal winds are the principal agent for the Es layer formation, and for this reason, there are no significant modifications during the disturbed periods.

## 5. Conclusions

We performed a comprehensive study of the disturbed electric field influences in the Es layer formation during 20 magnetic storms. We analyzed the digisonde data and modeling results during the main and recovery phases of magnetic storms in three regions over the Brazilian sector, BV, SLZ, and CXP.

As a case study, we analyzed the Saint Patrick's magnetic storm event. We observed a clear relationship between the anomalous Es layers and the disturbance dynamo in BV. The same finding was statistically verified in the other 20 events studied here. Therefore, this work confirms that the Es layer behavior is strongly affected by the zonal DDEF in this region. This correlation is very important since the presence of a strong Es layer in the ionograms at BV can be an indicator of the DDEF when the TEC data is not available.

Over SLZ, we noticed that the electric field has an influence on the Es layer formation during the main phase of the magnetic storms. However, due to the low correlation between the electric field intensity and the Es layer density in the statistical analysis, we assumed that the EEJ current was still effective in SLZ even though this region is located near the magnetic equator influence border. In the ionograms on March 17, 2015, the  $Es_q$  and the  $Es_b$  layers occurred simultaneously. The magnetometer data reveals that the EEJ current was intensified during the main phase of this magnetic storm, reaching values high enough to develop the Gradient Drift instability structure. Thus, the irregularity layers were formed, leading to high  $fEs$  values.

The Es layer behavior in CXP was not influenced by the electric field at any phase of the magnetic storms. The wind shear mechanism was predominant, and therefore, the electric field played only a secondary role in the Es layer formation process. The only mechanism that could modify the Es layers over the CXP region is the particle precipitation during the disturbed times, as seen in previous works. However, we did not find any evidence of this mechanism in CXP, confirming that only the wind shear mechanism operated in our cases.

The results obtained from the theoretical model showed a good agreement with the observed Es layer formation over BV and CXP. The electric field threshold in BV is 2.5 mV/m, meaning that the numerical simulation provided satisfactory electron density for values lower than that. For higher values, the simulated Es

layer density becomes unrealistic. In CXP, the electric field variation in simulations caused few modifications in the Es layer formation, showing that tidal winds are dominant in this region. In this case, the maximum increase of the Es layer density was 55%, whereas the observational data showed an intensification of ~60% in most cases of this analysis. At last, MIRE did not provide satisfactory results when the electric field was included in SLZ. We credited these discrepancies to the fact that the EEJ effect is not yet modeled in MIRE.

Therefore, this study shows that the disturbed electric field can impact the Es layer formation at regions in the geographic/magnetic equator. We notice that the zonal eastward electric field in the main phase of the magnetic storm can cause an equatorial Es layer in SLZ, whereas it can weaken or not cause changes in the Es layer in regions such as BV and CXP. During the recovery phase, the zonal westward electric field contributes to forming the Es layer in BV. Finally, the electric field role in the Es layer dynamics in this work provides a significant contribution to our understanding of these competing mechanisms in the Es layer formation during disturbed periods.

### Data Availability Statement

The authors thank the High Altitude Observatory (HAO) of the National Center for Atmospheric Research (NCAR), in Colorado (<http://www.hao.ucar.edu/modeling/gswm/gswm.html>) for providing wind data used in MIRE model. The authors thank the OMNIWEB for providing IMF Bz, AE and Dst parameters used in the classification of the days and the GeoForschungsZentrum (GFZ) Potsdam for providing the list of geomagnetically quiet days (<http://wdc.kugi.kyoto-u.ac.jp/qddays/index.html>). The Digisonde data from Boa Vista, São Luís and Cachoeira Paulista, TEC data, and Magnetometer data can be downloaded upon registration at the Embrace webpage from INPE Space Weather Program in the following link: <http://www2.inpe.br/climaespacial/portal/en/>.

### Acknowledgments

L. C. A. Resende would like to thank the China-Brazil Joint Laboratory for Space Weather (CBJLSW), National Space Science Center (NSSC), Chinese Academy of Sciences (CAS) for supporting her postdoctoral. J. Shi would like to thank the National Natural Science Foundation of China (grant 42074201 and 41674145) and the Specialized Research Fund for State Key Laboratory in China. C. M. Denardini thanks CNPq/MCTI, grant 03121/2014-9. I. S. Batista thanks CNPq/MCTI, grants 405555/2018-0 and 306844/2019-2. G. A. S. Picanço thanks CAPES/MEC (grant 88887.467444/2019-00). V. F. Andrioli and J. Moro would like to thank the CBJLSW/NSSC/CAS for supporting their postdoctoral. J. Moro would like to thank CNPq/MCTIC (grant 429517/2018-01) and the CBJLSW-NSC/CAS for supporting his postdoctoral. R. P. Silva thanks CNPq/MCTI (grant 300986/2020-3). D. Barros thanks CNPq/MCTI, grant 300974/2020-5. S. S. Chen thanks CAPES/MEC (grant 88887.362982/2019-00).

### References

- Abdu, M. A. (2005). Equatorial ionosphere–thermosphere system: Electrodynamic and irregularities. *Advances in Space Research*, 35(5), 771–787. <https://doi.org/10.1016/j.asr.2005.03.150>
- Abdu, M. A., Batista, I. S., Brum, G. M., MacDougall, J. W., Santos, A. M., de Souza, J. R., & Sobral, J. H. A. (2010). Solar flux effects on the equatorial evening vertical drift and meridional winds over Brazil: A comparison between observational data and the IRI model and the HWM representations. *Advances in Space Research*, 46(8), 1078–1085. <https://doi.org/10.1016/j.asr.2010.06.009>
- Abdu, M. A., & Brum, G. M. (2009). Electrodynamic of the vertical coupling processes in the atmosphere–ionosphere system of the low latitude region. *Earth Planets and Space*, 61, 385–395. <https://doi.org/10.1186/BF03353156>
- Abdu, M. A., de Souza, J. R., Batista, I. S., Santos, M. A., Sobral, J. H. A., Rastogi, R. G., & Chandra, H. (2014). The role of electric fields in sporadic E layer formation over low latitudes under quiet and magnetic storm conditions. *Journal of Atmospheric and Terrestrial Physics*, 115, 95–105. <https://doi.org/10.1016/j.jastp.2013.12.003>
- Abdu, M. A., de Souza, J. R., Sobral, J. H. A., & Batista, I. S. (2006). Magnetic storm associated disturbance dynamo effects in the low and equatorial latitude ionosphere, in recurrent magnetic storms: Corotating solar wind streams. *Geophysical Monograph Series*, 167, 283–304. <https://doi.org/10.1029/167GM22>
- Abdu, M. A., MacDougall, J. W., Batista, I. S., Sobral, J. H. A., & Jayachandran, P. T. (2003). Equatorial evening prereversal electric field enhancement and sporadic E layer disruption: A manifestation of E and F region coupling. *Journal of Geophysical Research*, 108(A6), 1–12. <https://doi.org/10.1029/2002JA009285>
- Astafyeva, E., Zakharenkova, I., & Förster, M. (2015). Ionospheric response to the 2015 St. Patrick's Day storm: A global multi-instrumental overview. *Journal of Geophysical Research: Space Physics*, 120(10), 9023–9037. <https://doi.org/10.1002/2015JA021629>
- Batista, I. S., & Abdu, M. A. (1977). Magnetic storm delayed sporadic E enhancements in the Brazilian geomagnetic anomaly. *Journal of Geophysical Research*, 82, 4777–4783. <https://doi.org/10.1029/JA082i029p04777>
- Batista, I. S., Candido, C. M. N., Souza, J. R., Abdu, M. A., Araujo, R. C., Resende, L. C. A., & Santos, A. M. (2017). F3 layer development during quiet and disturbed periods as observed at conjugate locations in Brazil: The role of the meridional wind. *Journal of Geophysical Research: Space Physics*, 122(2), 2361–2373. <https://doi.org/10.1002/2016JA023724>
- Batista, I. S., Diogo, E. M., Souza, J. R., Abdu, M. A., & Bailey, G. J. (2011). *Equatorial ionization anomaly: The role of thermospheric winds and the effects of the geomagnetic field secular variation*. Aeronomy of the Earth's atmosphere and ionosphere, 1ed. (Vol. 2, pp. 317–328). Springer. [https://doi.org/10.1007/978-94-007-0326-1\\_23](https://doi.org/10.1007/978-94-007-0326-1_23)
- Bittencourt, J. A., & Abdu, M. A. (1981). A theoretical comparison between apparent and real vertical ionization drift velocities in the equatorial F region. *Journal of Geophysical Research*, 86(A4), 2451–2454. <https://doi.org/10.1029/JA086iA04p02451>
- Blagoveshchensky, D. V., & Sergeeva, M. A. (2020). Ionospheric parameters in the European sector during the magnetic storm of August 25–26, 2018. *Advances in Space Research*, 65, 11–18. <https://doi.org/10.1016/j.asr.2019.07.044>
- Blanc, M., & Richmond, A. D. (1980). The ionospheric disturbance dynamo. *Journal of Geophysical Research*, 85(A4), 1669–1686. <https://doi.org/10.1029/JA085iA04p01669>
- Carrasco, A. J., Batista, I. S., & Abdu, M. A. (2007). Simulation of the sporadic E layer response to pre-reversal associated evening vertical electric field enhancement near dip equator. *Journal of Geophysical Research*, 112(A06), 324–335. <https://doi.org/10.1029/2006JA012143>

- Chandra, H., & Rastogi, R. (1975). Blanketing sporadic E layer near the magnetic equator. *Journal of Atmospheric and Terrestrial Physics*, 80(1), 149–153. <https://doi.org/10.1029/JA080i001p00149>
- Conceição-Santos, F., Muella, M. T. A. H., Resende, L. C. A., Fagundes, P. R., Andrioli, V. F., Batista, P. P., et al. (2019). Occurrence and modeling examination of Sporadic-E layers in the region of the South America (Atlantic) magnetic anomaly. *Journal of Geophysical Research: Space Physics*, 124(11), 9676–9694. <https://doi.org/10.1029/2018JA026397>
- De Michelis, P., Pignalberi, A., Consolini, G., Coco, I., Tozzi, R., Pezzopane, M., & Balasis, G. (2020). On the 2015 St. Patrick storm turbulent state of the ionosphere: Hints from the Swarm mission. *Journal of Geophysical Research: Space Physics*, 125, e2020JA027934. <https://doi.org/10.1029/2020ja027934>
- Denardini, C. M., Abdu, M. A., Aveiro, H. C., Resende, L. C. A., Almeida, P. D. S. C., Olivio, E. P. A., et al. (2009). Counter electrojet features in the Brazilian sector: simultaneous observation by radar, digital sounder and magnetometers. *Annales Geophysicae*, 27, 1593–1603. <https://doi.org/10.5194/angeo-27-1593-2009>
- Denardini, C. M., Picanço, G. A. S., Barbosa Neto, P. F., Nogueira, P. A. B., Carmo, C. S., Resende, L. C. A., et al. (2020). Ionospheric scale index map based on TEC data for space weather studies and applications. *Space Weather*, 18, e2019SW002328. <https://doi.org/10.1029/2019SW002328>
- Denardini, C. M., Resende, L. C. A., Moro, J., & Chen, S. S. (2016). Occurrence of the blanketing sporadic E layer during the recovery phase of the October 2003 superstorm. *Earth, Planets and Space*, 80(68), 1–9. <https://doi.org/10.1186/s40623-016-0577-z>
- Devasia, C. V., Sreeja, V., & Ravindran, S. (2006). Solar cycle dependent characteristics of the equatorial blanketing Es layers and associated irregularities. *Annales Geophysicae*, 24(11), 2931–2947. <https://doi.org/10.5194/angeo-24-2931-2006>
- Fejer, B. G., Larsen, M. F., & Farley, D. T. (1983). Equatorial disturbance dynamo electric fields. *Geophysical Research Letters*, 10(7), 537–540. <https://doi.org/10.1029/GL010i007p00537>
- Fejer, B. G., & Scherliess, L. (1995). Time dependent response of equatorial ionospheric electric fields to magnetospheric disturbances. *Geophysical Research Letters*, 22, 851–854. <https://doi.org/10.1029/95gl00390>
- Forbes, J. M. (1981). The equatorial electrojet. *Reviews of Geophysics*, 19(3), 469–504. <https://doi.org/10.1029/RG019i003p00469>
- Forbes, J. M., Roble, R. G., & Marcos, F. A. (1995). Equatorial penetration of magnetic disturbance effects in the thermosphere and ionosphere. *Journal of Atmospheric and Terrestrial Physics*, 57(10), 1085–1093. [https://doi.org/10.1016/0021-9169\(94\)00124-7](https://doi.org/10.1016/0021-9169(94)00124-7)
- Gonzalez, W. D., Joselyn, J. A., Kamide, Y., Kroehl, H. W., Rostoker, G., Tsurutani, B. T., & Vasyliunas, V. M. (1994). What is a magnetic storm?. *Journal of Geophysical Research*, 99(A4), 5771–5792. <https://doi.org/10.1029/93JA02867>
- Hagan, M. E., & Forbes, J. M. (2002). Migrating and nonmigrating diurnal tides in the middle and upper atmosphere excited by tropospheric latent heat release. *Journal of Geophysical Research*, 107, ACL6. <https://doi.org/10.1029/2001JD001236>
- Haldoupis, C. (2011). A tutorial review on Sporadic E layers. *Aeronomy of the Earth's Atmosphere-Ionosphere*, 29(2), 381–394. [https://doi.org/10.1007/978-94-007-0326-1\\_29](https://doi.org/10.1007/978-94-007-0326-1_29)
- Haldoupis, C., Meek, C., Christakis, N., Pancheva, D., & Bourdillon, A. (2006). Ionogram Height–Time–Intensity observations of descending sporadic E layers at mid-latitude. *Journal of Atmospheric and Terrestrial Physics*, 68, 539–557. <https://doi.org/10.1016/j.jastp.2005.03.020>
- Kelley, M. (1989). *The earth's ionosphere*. Academic Press. <https://doi.org/10.1016/B978-0-12-404013-7.X5001-1>
- Kopp, E. (1997). On the abundance of metal ions in the lower ionosphere. *Journal of Geophysical Research*, 102, 9667–9674.
- Layzer, D. (1972). Theory of midlatitude sporadic E. *Radio Science*, 7(3), 385–395. <https://doi.org/10.1029/RS007i003p00385>
- Manson, A. H., MeekHagan, C. M., Koshyk, J., FrankeFritts, S. D., Hall, C., Hocking, W., et al. (2002). Seasonal variations of the semi-diurnal and diurnal tides in the MLT: Multi-year MF radar observations from 2 to 70°N, modelled tides (GSWM, CMAM). *Annales Geophysicae*, 20, 661–677. <https://doi.org/10.5194/angeo-20-661-2002>
- Mathews, J. D. (1998). Sporadic E: current views and recent progress. *Journal of Atmospheric and Terrestrial Physics*, 60, 413–435. [https://doi.org/10.1016/S1364-6826\(97\)00043-6](https://doi.org/10.1016/S1364-6826(97)00043-6)
- Mathews, J. D., & Bekeny, F. S. (1979). Upper atmosphere tides and the vertical motion of ionospheric sporadic layers at Arecibo. *Journal of Geophysical Research*, 84(A6), 2743–2750. <https://doi.org/10.1029/JA084iA06p02743>
- Maurya, A. K., Venkatesham, K., Kumar, S., Singh, R., Tiwari, P., & Singh, A. K. (2018). Effects of St. Patrick's Day geomagnetic storm of March 2015 and of June 2015 on low-equatorial D region ionosphere. *Journal of Geophysical Research: Space Physics*, 123(8), 6836–6850. <https://doi.org/10.1029/2018JA025536>
- Moro, J., Denardini, C. M., Resende, L. C. A., Chen, S. S., & Schuch, N. J. (2016). Equatorial E region electric fields at the dip equator: 2. Seasonal variabilities and effects over Brazil due to the secular variation of the magnetic equator. *Journal of Geophysical Research: Space Physics*, 121(10), 10231–10240. <https://doi.org/10.1002/2016JA022753>
- Moro, J., Resende, L. C. A., Denardini, C. M., Xu, J., Batista, I. S., Andrioli, V. F., & Schuch, N. J. (2017). Equatorial E region electric fields and sporadic E layer responses to the recovery phase of the November 2004 geomagnetic storm. *Journal of Geophysical Research: Space Physics*, 122, 12517–12533. <https://doi.org/10.1002/2017JA024734>
- Nogueira, P. A. B., Abdu, M. A., Batista, I. S., & Siqueira, P. M. (2011). Equatorial ionization anomaly and thermospheric meridional winds during two major storms over Brazilian low latitudes. *Journal of Atmospheric and Solar-Terrestrial Physics*, 73, 1535–1543. <https://doi.org/10.1016/j.jastp.2011.02.008>
- Otsuka, Y., Ogawa, T., Saito, A., Tsugawa, T., Fukao, S., & Miyazaki, S. (2002). A new technique for mapping of total electron content using GPS network in Japan. *Earth Planets and Space*, 54, 63–70. <https://doi.org/10.1186/BF03352422>
- Pancheva, D., Haldoupis, C., Meek, C. E., Manson, A. H., & Mitchell, N. J. (2003). Evidence of a role for modulated atmospheric tides in the dependence of sporadic E layers on planetary waves. *Journal of Geophysical Research*, 108(A5), 1176. <https://doi.org/10.1029/2002JA009788>
- Pignalberi, A., Pezzopane, M., & Zuccheretti, E. (2014). Sporadic E layer at mid-latitudes: average properties and influence of atmospheric tides. *Annales Geophysicae*, 32(11), 1427–1440. <https://doi.org/10.5194/angeo-32-1427-2014>
- Prasad, S. N. V. S., Prasad, D. S. V. V. D., Venkatesh, K. K., Niranjan, K., & Rama Rao, P. V. S. (2012). Diurnal and seasonal variations in sporadic E-layer (Es layer) occurrences over equatorial, low and mid latitude stations—A comparative study. *Indian Journal of Radio and Space Physics*, 41, 26–35.
- Rastogi, R. G., Chandra, H., Condori, L., Abdu, M. A., Reinisch, B., Tsunoda, R. T., et al. (2012). Abnormally large magnetospheric electric field on 9 November 2004 and its effect on equatorial ionosphere around the world. *Journal of Earth System Science*, 121(5), 1145–1161. <https://doi.org/10.1007/s12040-012-0231-5>
- Reinisch, B. W., Galkin, I. A., & Khmyrov, G. M. (2009). The new Digisonde for research and monitoring applications. *Radio Science*, 44, RS0A24. <https://doi.org/10.1029/2008RS004115>
- Reinisch, B. W., Galkin, I. A., Khmyrov, G. M., Kozlov, A., & Kitrosser, D. (2004). Automated collection and dissemination of ionospheric data from the digisonde network. *Advances in Radio Science*, 2, 241–247. <https://doi.org/10.5194/ars-2-241-2004>



- Resende, L. C. A., Batista, I. S., Denardini, C. M., Batista, P. P., Carrasco, A. J., Andrioli, V. F., & Moro, J. (2017a). Simulations of blanketing sporadic E-layer over the Brazilian sector driven by tidal winds. *Journal of Atmospheric and Solar-Terrestrial Physics*, *154*, 104–114. <https://doi.org/10.1016/j.jastp.2016.12.012>
- Resende, L. C. A., Batista, I. S., Denardini, C. M., Batista, P. P., Carrasco, A. J., Andrioli, V. F., & Moro, J. (2017b). The influence of tidal winds in the formation of blanketing sporadic E-layer over equatorial Brazilian region. *Journal of Atmospheric and Solar-Terrestrial Physics*, *171*, 64–67. <https://doi.org/10.1016/j.jastp.2017.06.009>
- Resende, L. C. A., Batista, I. S., Denardini, C. M., Carrasco, A. J., Andrioli, V. F., Moro, J., et al. (2016). Competition between winds and electric fields in the formation of blanketing sporadic E layers at equatorial regions. *Earth Planets and Space*, *68*, 201. <https://doi.org/10.1186/s40623-016-0577-z>
- Resende, L. C. A., & Denardini, C. M. (2012). Equatorial sporadic E-layer abnormal density enhancement during the recovery phase of the December 2006 magnetic storm: A case study. *Earth Planet Space*, *64*, 345–351. <https://doi.org/10.5047/eps.2011.10.007>
- Resende, L. C. A., Denardini, C. M., & Batista, I. S. (2013). Abnormal fbEs enhancements in equatorial Es layers during magnetic storms of solar cycle 23. *Journal of Atmospheric and Solar-Terrestrial Physics*, *102*, 228–234. <https://doi.org/10.1016/j.jastp.2013.05.020>
- Resende, L. C. A., Shi, J., Denardini, C. M., Batista, I. S., Nogueira, P. A. B., Andrioli, V. F., et al. (2020). The influence of disturbance dynamo electric field in the formation of strong sporadic E Layers over Boa Vista, a low-latitude station in the American Sector. *Journal of Geophysical Research: Space Physics*, *125*(7), e2019JA027519. <https://doi.org/10.1029/2019ja027519>
- Rishbeth, H., Ganguly, S., & Walker, J. C. G. (1978). Field-aligned and field-perpendicular velocities in ionospheric F2-layer. *Journal of Atmospheric and Solar-Terrestrial Physics*, *40*(7), 767–784. [https://doi.org/10.1016/0021-9169\(78\)90028-4](https://doi.org/10.1016/0021-9169(78)90028-4)
- Spogli, L., Cesaroni, C., Mauro, D. D., Pezzopane, M., Alfonsi, L., Musico, E., et al. (2016). Formation of ionospheric irregularities over Southeast Asia during the 2015 St. Patrick's Day storm. *Journal of Geophysical Research: Space Physics*, *121*, 12211–12233. <https://doi.org/10.1002/2016JA023222>
- Takahashi, H., Costa, S., Otsuka, Y., Shiokawa, K., Monico, J. F. G., Paula, E., et al. (2014). Diagnostics of equatorial and low latitude ionosphere by TEC mapping over Brazil. *Advances in Space Research*, *54*, 385–394. <https://doi.org/10.1016/j.asr.2014.01.032>
- Takahashi, H., Wrasse, C. M., Denardini, C. M., Pádua, M. B., de Paula, E. R., Costa, S. M. A., et al. (2016). Ionospheric TEC weather map over south America. *Space Weather*, *14*, 937–949. <https://doi.org/10.1002/2016SW001474>
- Tsurutani, B. T., Verkhoglyadova, O. P., Mannucci, A. J., Saito, A., Araki, T., Yumoto, K., et al. (2008). Prompt penetration electric fields (PPEFs) and their ionospheric effects during the great magnetic storm of 30–31 October 2003. *Journal of Geophysical Research: Space Physics*, *113*, 1–10, A05311. <https://doi.org/10.1029/2007JA012879>
- Tulasi Ram Nilam, S. B., Balan, N., Zhang, Q., Shiokawa Chakrabarty, K. D., Xing, Z., Venkatesh, K., et al. (2019). Three different episodes of prompt equatorial electric field perturbations under steady southward IMF Bz during St. Patrick's day storm. *Journal of Geophysical Research: Space Physics*, *124*, 10428–10443. <https://doi.org/10.1029/2019JA027069>
- Venkatesh, K., Patra, A. K., Balan, N., Fagundes, P. R., Tulasi Ram, S., Batista, I. S., & Reinisch, B. W. (2019). Superfountain effect linked with 17 March 2015 geomagnetic storm manifesting distinct F3 layer. *Journal of Geophysical Research: Space Physics*, *124*, 6127–6137. <https://doi.org/10.1029/2019JA026721>
- Venkatesh, K., Tulasi Ram, S., Fagundes, P. R., Seemala, G. K., & Batista, I. S. (2017). Electrodynamical disturbances in the Brazilian equatorial and low-latitude ionosphere on St. Patrick's Day storm of 17 March 2015. *Journal of Geophysical Research: Space Physics*, *122*(4), 4553–4570. <https://doi.org/10.1002/2017JA024009>
- Whitehead, J. (1961). The formation of the Sporadic-E in the temperate zones. *Journal of Atmospheric and Terrestrial Physics*, *20*(1), 1155–1167. [https://doi.org/10.1016/0021-9169\(61\)90097-6](https://doi.org/10.1016/0021-9169(61)90097-6)
- Wu, C. C., Liou, K., Lepping, R. P., Hutting, L., Plunkett, S., Howard, R. A., & Socker, D. (2016). The first super geomagnetic storm of solar cycle 24: “The St. Patrick's Day event (17 March 2015)”. *Earth, Planets and Space*, *68*(1), 151–163. <https://doi.org/10.1186/s40623-016-0525-y>
- Yadav, S., Sunda, S., & Sridharan, R. (2016). The impact of the 17 March 2015 St. Patrick's Day storm on the evolutionary pattern of equatorial ionization anomaly over the Indian longitudes using high-resolution spatiotemporal TEC maps: New insights. *Space Weather*, *14*, 786–801. [doi:10.1002/2016SW001408](https://doi.org/10.1002/2016SW001408)
- Zhang, S.-R., Zhang, Y., Wang, W., & Verkhoglyadova, O. P. (2017). Geospace system responses to the St. Patrick's Day storms in 2013 and 2015. *Journal of Geophysical Research: Space Physics*, *122*, 6901–6906. <https://doi.org/10.1002/2017JA024232>